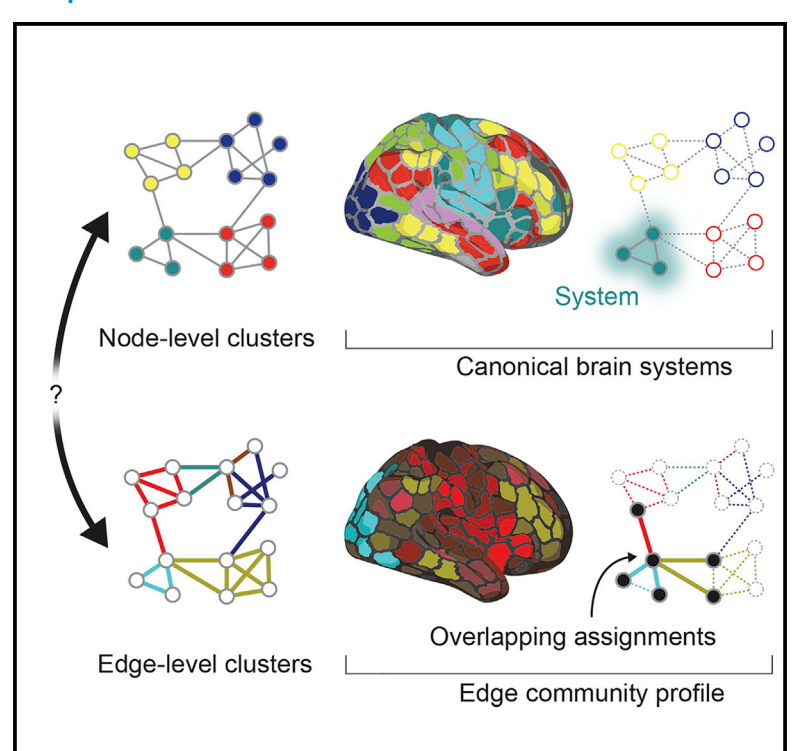
The diversity and multiplexity of edge communities within and between brain systems

Graphical abstract



Authors

Youngheun Jo, Farnaz Zamani Esfahlani, Joshua Faskowitz, Evgeny J. Chumin, Olaf Sporns, Richard F. Betzel

Correspondence

rbetzel@indiana.edu

In brief

Jo et al. detect pervasively overlapping communities in functional brain networks. They classify overlapping communities based on how those communities link sensorimotor and heteromodal systems. Focusing on the control network, they highlight three overlapping community profiles, revealing putative communication pathways with other systems and the rest of the neocortex.

Highlights

- Edge-centric methods reveal overlapping community structure in functional brain networks
- Clustering regions based on community similarity reveals putative communication paths
- The number of clusters is greater in heteromodal systems compared with sensorimotor systems
- Overlapping community structure is stable within an individual across repeated scans







Article

The diversity and multiplexity of edge communities within and between brain systems

Youngheun Jo,¹ Farnaz Zamani Esfahlani,¹ Joshua Faskowitz,¹,² Evgeny J. Chumin,¹,³ Olaf Sporns,¹,2,3,4 and Richard F. Betzel¹,2,3,4,5,*

SUMMARY

The human brain is composed of functionally specialized systems that support cognition. Recently, we proposed an edge-centric model for detecting overlapping communities. It remains unclear how these communities and brain systems are related. Here, we address this question using data from the Midnight Scan Club and show that all brain systems are linked via at least two edge communities. We then examine the diversity of edge communities within each system, finding that heteromodal systems are more diverse than sensory systems. Next, we cluster the entire cortex to reveal it according to the regions' edge-community profiles. We find that regions in heteromodal systems are more likely to form their own clusters. Finally, we show that edge communities are personalized. Our work reveals the pervasive overlap of edge communities across the cortex and their relationship with brain systems. Our work provides pathways for future research using edge-centric brain networks.

INTRODUCTION

The human brain is a complex network made up of functionally and structurally interacting neural elements (Bullmore and Sporns, 2009; Bassett and Sporns, 2017; Park and Friston, 2013). Traditionally, brain networks are represented using models in which nodes and edges are defined as regions and the magnitude of their correlated activity, i.e., functional connectivity (FC), respectively (Friston et al., 1993; Rogers et al., 2007; Craddock et al., 2013). This node-centric model emphasizes interactivity among pairs of nodes and has been especially useful in cognitive and network neuroscience, where inter-individual variation has been linked to subjects' cognitive (Shirer et al., 2012), disease (Fornito et al., 2015), and developmental states (Di Martino et al., 2014).

Among the most salient features of node-centric functional networks is their decomposability into subnetworks called "modules" or "communities" (Power et al., 2011; Thomas Yeo et al., 2011; Meunier et al., 2010; Sporns and Betzel, 2016). In general, networks with modular structure are evolvable (Kirschner and Gerhart, 1998; Kashtan and Alon, 2005), are capable of supporting complex dynamics (Hizanidis et al., 2016), can buffer perturbations, and can facilitate cost-effective embedding in three-dimensional space (Bassett et al., 2010). In the case of human brain networks, the boundaries of modules delineate patterns of task-evoked activity (Smith et al., 2009) and correspond closely with known cognitive and functional systems (Power

et al., 2011; Thomas Yeo et al., 2011). This is true even when modules are estimated under task-free or resting-state conditions. This observation has prompted the hypothesis that modular structure is a key feature for supporting specialized brain function (Bertolero et al., 2015).

In virtually every application, the brain's modular structure is estimated using node-centric functional connectivity, which results in a mapping of nodes (brain regions) to modules (Fortunato, 2010). Recently, we proposed an edge-centric model for representing pairwise functional interactions among a network's edges (Faskowitz et al., 2020; Zamani Esfahlani et al., 2020b). Although node (nFC) and edge FC (eFC) are generated from identical fMRI time series, the two constructs provide complementary insight into brain network organization and operation. Whereas nFC measures the extent to which the activity of one brain region fluctuations with the activity of another, eFC unwraps those co-fluctuations across time, first yielding momentby-moment accounts of the co-fluctuations between pairs of brain regions (edges) and then assessing the similarity between pairs of co-fluctuation time series (Zamani Esfahlani et al., 2020b).

Intuitively, if one considers nFC as a measure of communication between pairs of brain regions (Reid et al., 2019), eFC works by first unwrapping that communication pattern, generating time-varying accounts of the "conversation" between every pair of brain regions. It then compares pairs of conversations to one another, calculating their pairwise similarity. In other



¹Department of Psychological and Brain Sciences, Indiana University, Bloomington, IN 47405, USA

²Program in Neuroscience, Indiana University, Bloomington, IN 47405, USA

³Network Science Institute, Indiana University, Bloomington, IN 47405, USA

⁴Cognitive Science Program, Indiana University, Bloomington, IN 47405, USA

⁵Lead contact

^{*}Correspondence: rbetzel@indiana.edu https://doi.org/10.1016/j.celrep.2021.110032



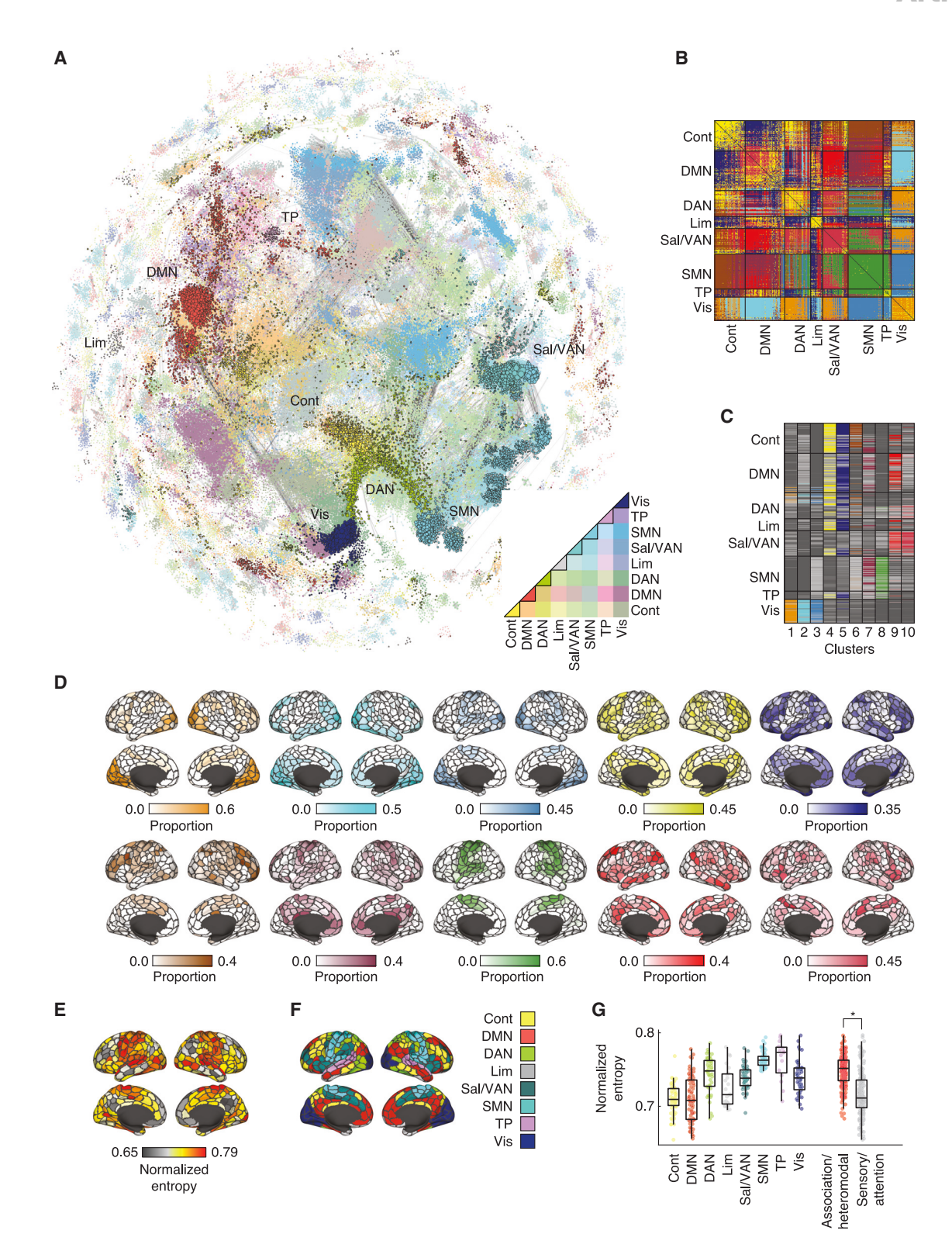


Figure 1. Edge functional connectivity

(A) Force-directed layout of edge functional connectivity (eFC). Each point represents an individual edge, colored according to the brain systems to which the edge's stub nodes belong to.

(B) Edge communities mapped into a node × node matrix. Each color reflects a distinct edge community.

(legend continued on next page)

Article



words, eFC measures whether there are similar conversations taking place in the brain (Uddin, 2020).

Similarly, compared with the modular structure of nFC, the modules estimated from eFC provide complementary information about the brain's system-level organization. Clustering nFC results in a partition of nodes into non-overlapping modules, such that each brain region gets assigned to one community and one community only (Newman and Girvan, 2004; Rosvall and Bergstrom, 2008). Applying the same algorithm to eFC results in a non-overlapping partition of edges into communities. However, when edges are mapped back to their respective nodes, non-overlapping edge partitions yield overlapping nodal partitions, such that a single node can be associated with multiple communities (Ahn et al., 2010; Evans and Lambiotte, 2009).

In a previous paper, we characterized the basic properties of eFC, including its modular structure (Faskowitz et al., 2020). However, the relationship between modules derived from eFC and brain systems derived from nFC remains unclear. Are the edges that link brain systems to one another homogeneous in terms of their edge community assignments, or are brain systems linked to one another via diverse assemblies of edges that comprise several distinct edge communities (Vaiana and Muldoon, 2020; De Domenico, 2017)? Addressing these questions would add clarity to our understanding of how the brain's modular structure helps support cognition.

Here, we investigate this relationship in greater detail with eFC estimated using Midnight Scan Club data (MSC) (Gratton et al., 2018; Gordon et al., 2017b). First, we derive edge communities and show that individual brain regions participate in many different communities. Next, we investigate how these communities are distributed within and between traditionally defined brain systems. We demonstrate that all systems are linked to one another via multiple distinct edge communities. Focusing on the configuration of edge communities within brain systems, we use a data-driven community-detection algorithm to uncover their multi-scale organization (Betzel and Bassett, 2017), demonstrating that higher-order cognitive systems exhibit more complex communities compared with sensorimotor systems. We then apply the same clustering algorithm to data from the entire cerebral cortex, identifying a novel cluster structure that deviates, systematically, from previously described brain systems. Finally, we investigate edge community structure at the level of individual subjects. We show that edge community structure exhibits remarkable idiosyncrasies, which are driven by the personalization of edge communities outside of sensorimotor cortices. The results presented here offer pathways for future studies aimed at relating features of edge-centric networks to individual differences in behavior and cognition.

RESULTS

In this section, we present analyses of eFC estimated using resting-state data from the MSC. Specifically, we analyzed parcel time series from N = 400 regions (Schaefer et al., 2018). We calculated eFC by first Z-scoring each regional time series and computing the element-wise product between all pairs of time series, yielding M = 79,800 unique pairs corresponding to every possible edge. Using these so-called edge time series (Zamani Esfahlani et al., 2020b, 2021a; Betzel et al., 2021; Greenwell et al., 2021; Faskowitz et al., 2020), we calculated the 79,800 × 79,800 eFC matrix of all pairwise similarities (see STAR Methods for details). This procedure was repeated separately for each of the 10 subjects in the MSC and for each of their 10 scans. At times, we find it useful to create composite eFC matrices, both at the group level, by averaging over subjects and scans, but also at the subject level, by averaging over scans. Complete details of MRI acquisition, pre-processing pipelines, and network construction can be found in STAR Methods.

Edge communities reveal overlapping network structure

Many studies have shown that the brain exhibits modular structure, meaning that its elements can be partitioned into cohesive clusters called "communities" or "modules" (Power et al., 2011; Thomas Yeo et al., 2011; Betzel et al., 2018b, 2017). Modules are usually defined to be internally dense and non-overlapping (with some notable exceptions; Najafi et al., 2016; Thomas Yeo et al., 2014; Faskowitz et al., 2018; Betzel et al., 2018a), such that nodes are assigned to one module only, and that nodes tend to be strongly connected to other nodes in their own module and weakly connected to nodes in other modules. Recently, we developed an edge-centric representation of brain networks (see Figure 1A for an example of eFC drawn using a forcedirected layout algorithm), which we used to cluster network edges, resulting in overlapping nodal communities. Here, we replicate those findings using data from the MSC. We show that community overlap varies across cerebral cortex and canonical brain systems (Schaefer et al., 2018). These observations motivate a further exploration of the relationship of brain systems and edge communities.

We first derived group-representative edge communities. To do so, we estimated the edge-time series for all 100 resting-state scans in the dataset (10 subjects; 10 scans each; see Figure S1 in which we compare select properties of edge-time series to time-varying FC estimated using sliding windows), concatenated those data, and used a two-stage k-means clustering algorithm to generate 250 estimates of communities, before synthesizing those results into consensus edge communities. Here,

⁽C) Edge communities mapped back to individual nodes. In this plot, rows and columns represent nodes and communities, respectively. Within each column, colors indicate the fraction of a node's edges that are associated with the corresponding edge community. We can project the columns of this matrix onto the

⁽D) Projections for each of the k = 10 edge communities. Line thickness is linearly proportional to mean connection weight. From edge communities, we can also calculate the normalized entropy for each node—a measure of community overlap.

⁽E) Projections of the overlap scores in (D) onto the cortical surface.

⁽F and G) We can then aggregate, entropy (overlap) scores according to brain systems. As in our previous paper, we find that overlap is greatest in primary sensory and attentional systems and lowest in association cortices. Asterisk indicates p < 10⁻³.



communities correspond to groups of edges (region pairs) whose co-activity over time follows a similar trajectory. These communities can be visualized in several different ways. First, because the clustering algorithm operates at the level of edges, we can visualize edge communities in matrix form, by labeling the edge between nodes i and j according to its edge community assignment (Figure 1B). Here, each color corresponds to a different edge community (as in our previous paper, we show results with the number of communities fixed at k = 10; see Figure S2A, for edge communities detected at other k values, and Figure S2B, for a comparison against a null model). A second strategy for visualizing edge communities is to calculate, for each node, the fraction of its edges that belongs to a given community. This procedure is especially useful because it allows us to describe edge communities more intuitively in terms of brain regions and systems (Figure 1C). This also allows us to visualize the topography of edge communities in anatomical space by projecting regional participation in edge communities onto brain surfaces (Figure 1D).

Following our previous paper, we then calculated the level of community overlap for a given brain region as normalized entropy, where values close to 0 indicate that a brain regions' edges are concentrated among a small number of communities, whereas values close to 1 indicate that edges are uniformly distributed over communities (Figure 1E). Specifically, normalized entropy was calculated for each brain region by first calculating how many of its edges were assigned to each of the k communities. Normalized entropy is simply the entropy over that distribution (see STAR Methods for more details). Notably, we found that there were no regions with entropies near zero, in agreement with the observation from our previous paper that brains exhibit "pervasive overlap." Nonetheless, the community overlap measure exhibited cortical specificity. Again, in agreement with our previous paper, we found that the greatest levels of overlap were concentrated in primary sensory and attentional networks Figures 1F and 1G). Specifically, we partitioned brain systems into two groups: a sensory-attention group comprising somatomotor, visual, dorsal attention, and the salience/ventral attention networks (220 regions); and a heteromodal group comprising control, default mode, limbic, and temporoparietal networks (180 regions). We compared the difference in mean entropy between groups and compared that value against a null distribution generated using a spatially constrained permutation of system labels (Váša et al., 2018). We found that the entropy of the sensory-attention group was greater than that of the heteromodal group (p < 10^{-3} ; 1,000 permutations; Figure 1G). This observation indicates that the connections associated with brain regions in those systems are involved in many different edge communities. In contrast, heteromodal association cortices, which include control, default mode, and limbic networks, exhibited the lowest levels of overlap. In the Supplementary material, we show that a significant amount of variance in those results can be partially anticipated from nFC alone (see Figure S3). These observations underscore the need for future work not only to assess more clearly the interrelationship between these two modalities (Novelli and Razi, 2021) but also to demonstrate that the unexplained variance is neurobiologically and/or behaviorally relevant.

Collectively, these results recapitulate the main findings from our previous paper (Faskowitz et al., 2020), and extend them to an increasingly fine-grained parcellation (Schaefer et al., 2018). More practically, the fact that we could obtain qualitatively similar community structure and overlap by clustering an edgetime series, which is more computationally tractable than the edge-connectivity matrix, makes it possible to perform additional complex analyses in the future. In summary, these findings are in line with our earlier report (Faskowitz et al., 2020) and provide a baseline for the following extension of the edge-connectivity framework.

System-level complexity of edge community structure

An edge community is a collection of edges—pairs of nodes whose co-fluctuations follow similar time courses. How are these communities distributed within and between canonical brain systems (Schaefer et al., 2018; Thomas Yeo et al., 2011; Power et al., 2011)? Are some brain systems linked to one another via many communities? Are others linked by few? Here, we address those questions by considering edge community templates-binarized maps of edge communities-which we aggregate into descriptions of system-level interactions. In general, we find additional evidence of "pervasive overlap" (Ahn et al., 2010), such that virtually all pairs of systems are linked to one another by at least two edge communities. We also find that, internally, sensorimotor systems are spanned by relatively few edge communities compared with that of higher-order heteromodal systems.

We first mapped edge community labels into a node-by-node matrix (Figure 2A) and, for each edge community, extracted its template pattern (Figure 2B), in which edges belonging to that community were assigned a value of 1, whereas all other edges were set equal to 0. We aggregated the nonzero elements in each template by cognitive systems, counting the fraction of the edges within or between those systems that belonged to a given edge community (Figure 2C). These system-by-system maps quantified the extent to which systems were linked by a given edge community (Figure 2D).

Using the system-by-system maps, we estimated the entropy associated with all pairs of systems (Figure 2E). Intuitively, if the edges between those systems belonged to a diverse set of edge communities, then the entropy score was high. On the other hand, if the edges belonged to relatively few communities, then the entropy was low. Interestingly, we found that the highest levels of entropy were associated with connections between the dorsal attention and cognitive control networks, whereas the lowest were associated with the within-system connections of the somatomotor network (Figures 2F and 2G). When considering just the internal edges of brain systems, we found that default mode and dorsal attention had the highest levels of entropy, whereas somatomotor, temporoparietal, and the visual network were among the lowest. We found similar patterns when considering the number of distinct edge communities observed in within- and between-system blocks (Figures 2H and 21).

Finally, we investigated the structure of each edge community in greater detail, focusing on the specific brain systems that it linked. Broadly, edge communities could be sub-divided into

Article



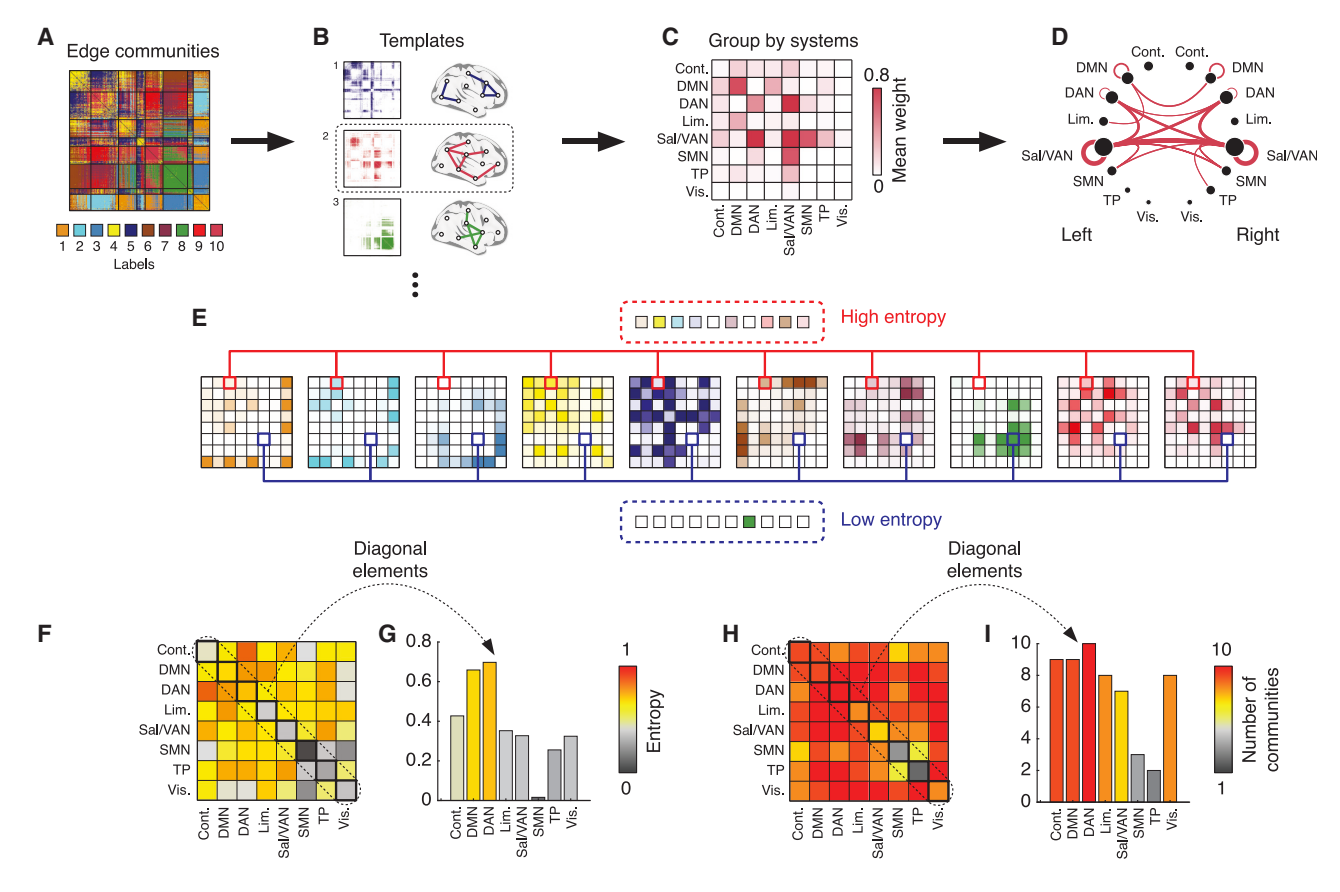


Figure 2. Edge community templates reveal system-dependent organization

- (A) Edge communities mapped into a node x node matrix.
- (B) We generated community templates, in which each community is represented as a binary matrix with edges assigned a value of 1 or 0, depending upon whether they were included in that community.
- (C) We aggregated template edges by brain systems and counting the number of edges that fell within or between eight canonical brain networks.
- (D) Each template describes the fraction of inter- and intra-system interactions mediated by a given edge community (here, we split systems into their left- and right-hemisphere components for visualization only).
- (E) We can use these templates to identify brain systems linked to one another by edges assigned to many or few edge communities (high or low entropy).
- (F) We calculated the entropies for all pairs of brain systems.
- (G-I) If we consider only within-system edges, we find that heteromodal association cortex tends to have greater entropy (G) and participate in a greater number of discrete edge communities than do primary sensory systems (H and I).

two groups: "cohesive" communities, which included disproportionately many within-system edges; and "bridge" communities, comprising mostly edges that fell between brain systems (Figure 3A). We further sub-classified "bridge" communities based on the systems that they linked: "association" bridges linked heteromodal systems (control, default mode, dorsal attention, limbic, salience/ventral attention, and temporoparietal systems) to one another, whereas "processing" bridges linked heteromodal and unimodal systems (somatomotor and visual) to each other (Figure 3B). As expected, we found that cohesive communities contained a greater proportion of within-system edges than bridge communities (Figure 3B; $p = 1.1 \times 10^{-4}$; t test with 10 samples). We also found that association communities contained a greater proportion of edges linking heteromodal systems to one another compared with that of processing communities (Figure 3C; p = 0.0019; t test with six samples) whereas processing communities contained a greater proportion of heteromodal to unimodal edges (Figure 3D; p = 1.4 x 10⁻⁴; t test with six samples). We show the full ontology of edge communities in Figure 3E. We find similar results with different numbers of edge communities (Figure S4).

Collectively, these findings suggest that the brain's edge community structure is pervasively overlapping, such that all pairs of brain systems are linked to one another via multiple edge communities, which, in turn, reflect distinct patterns of edge co-fluctuations. Second, these findings further suggest that, although all systems interact via distinct modes, the number and diversity of modes are system dependent and that heteromodal systems exhibit a more-complex internal structure than do sensorimotor systems. Further, the particular configuration of edge communities among brain systems suggests distinct functional classes, with some edge communities positioned to maintain the cohesiveness of systems and others to form links across system boundaries.



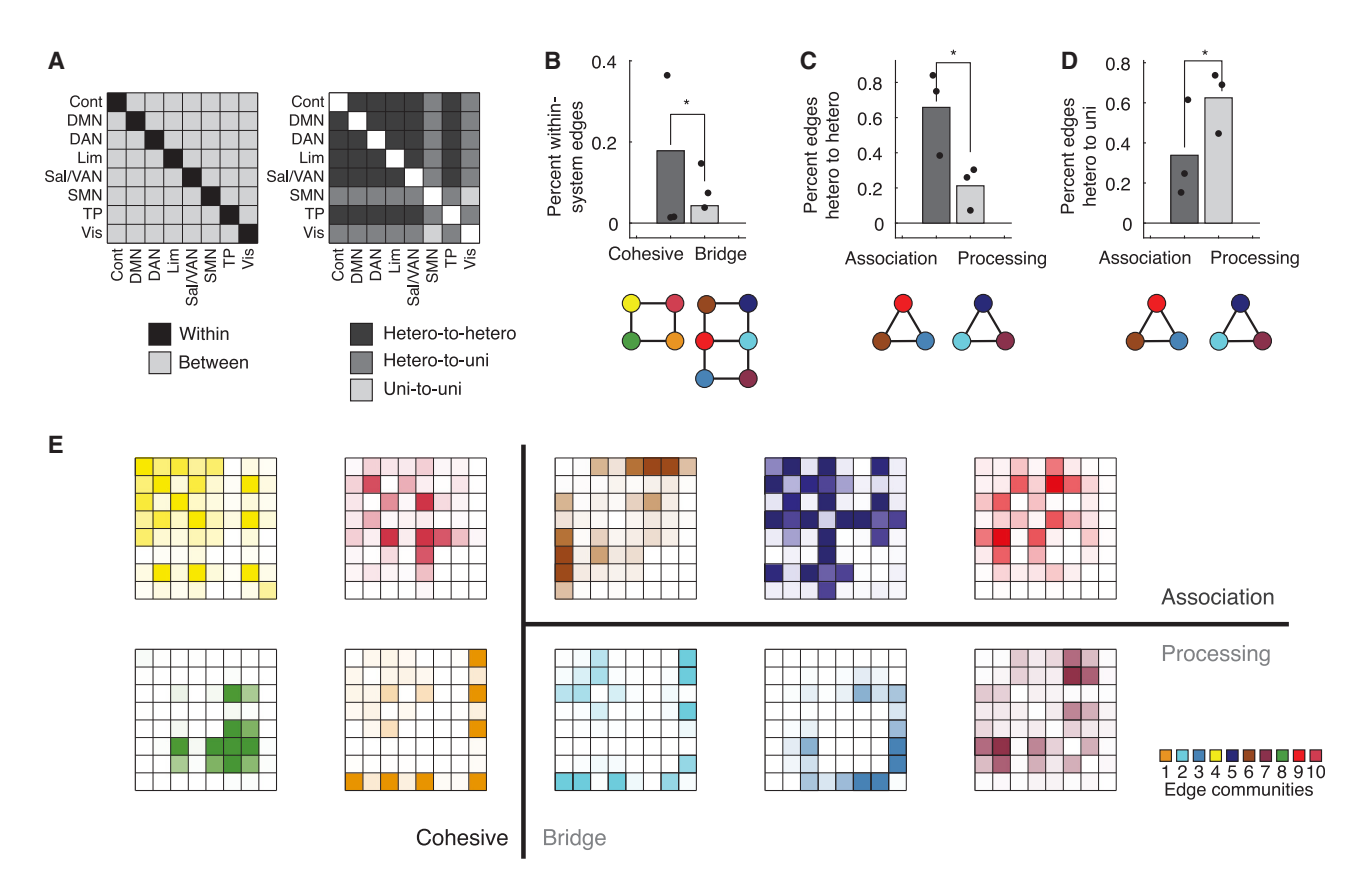


Figure 3. Categorization of edge communities

(A) Each edge community was classified as a "cohesive" or "bridge" community according to whether edges belonging to that community fell within or between brain systems, respectively. We further sub-classified bridge communities according to whether the edges linked heteromodal systems (control, default mode, dorsal attention, salience/ventral attention, limbic, and temporoparietal) to other heteromodal systems or to sensorimotor systems (somatomotor and visual). We referred to these two sub-categories as "association" and "processing" communities, respectively.

(B) As expected, we found that cohesive communities included a greater proportion within-system edges compared with bridge communities. Asterisk indicates $p = 1.1 \times 10^{-4}$.

(C and D) Similarly, association communities had a greater proportion of edges linking heteromodal systems to other heteromodal systems (C) whereas processing communities exhibited a greater proportion of heteromodal to unimodal edges (D). In (C), asterisk indicates p = 0.0019. In (D), asterisk indicates p = 1.4 x

(E) Ten edge communities divided into their respective classes. The vertical line divides "cohesive" from "bridge" communities, whereas the horizontal line divides "association" from "processing." The outlines (black, green, and red) are used to help identify system pairs responsible for that edge community's classification.

Multi-scale and system-dependent organization of edge community structure

In the System-level complexity of edge community structure, we showed that brain systems are linked to one another via different modes of coupling (edge communities). Notably, we found that the diversity of edge communities within brain systems was highly variable. Here, we investigate the internal structure of brain systems in greater detail. To do so, we introduce the concept of an "edge community profile" and define a measure of similarity for comparing profiles among pairs of regions. Separately, for each cognitive system, we generated the interregional similarity matrix among all regions assigned to that system, which we partitioned using multi-scale modularity maximization (Newman and Girvan, 2004; Reichardt and Bornholdt, 2006; Traag et al., 2011; Bazzi et al., 2016). Modularity maximization is a well-studied community-detection framework in which communities correspond to groups of nodes whose density of connections to one another maximally exceeds what would be expected by chance (Zamani Esfahlani et al., 2021b; Betzel, 2020). In this case, we search for communities of nodes whose edge community similarity is greater than that of a chance model (see STAR Methods for details). We find that the number of distinct subcommunities within each brain system was greatest for higherorder cognitive systems, whereas sensorimotor networks exhibited many fewer sub-communities. Note that, here, we switch clustering algorithms from k-means, which we used to cluster edge time series, to modularity maximization. This decision was motivated practically because the dimensionality of the edge-community similarity matrix was considerably less than that of the edge time series, which allowed us to use the more-computationally demanding modularity maximization. For completeness, we report the similarity of whole-brain

Article



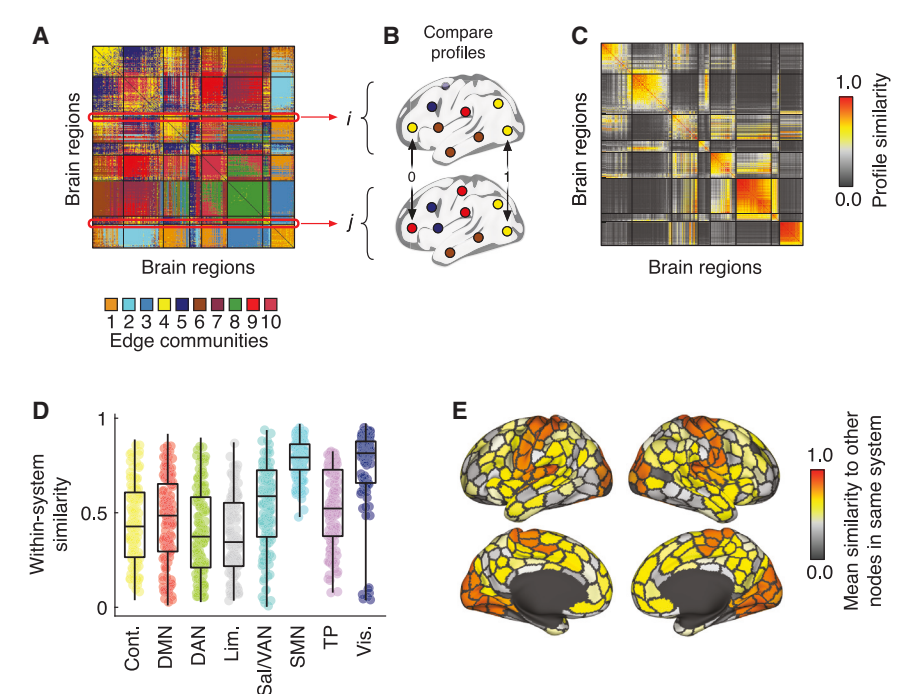


Figure 4. Edge community similarity

(A) Edge communities reshaped into a node x node matrix

(B) We can treat the columns and rows of this matrix as "profiles" for different regions and compare nodes' community labels to measure the similarity of two profiles with respect to one

(C and D) Repeating this process for all pairs of nodes results in a similarity matrix (C). The average similarity between nodes within each brain system is highly variable. We find that control networks exhibit low levels of overlap and are composed of nodes with heterogeneous edge community profiles (D); individual points in (D) correspond to the edge community similarity for pairs of brain regions within a given system. In contrast, we find that sensorimotor networks (visual + somatomotor) exhibit high levels of overlap but are composed of nodes with homogeneous edge community profiles.

(E) We can also visualize the heterogeneity of each system by projecting their mean internal similarity onto the cortex. Note that similarity is greatest for visual and somatomotor systems.

partitions detected using k-means and modularity maximization in the Supplementary material (Figures S2C and S2D).

To estimate the multi-scale community structure, we leveraged the node-by-node matrix representation of edge communities (Figure 4A) and extracted each region's edge-community profile as the corresponding row (Figure 4B). To measure the similarity between two regions' profiles, we simply measured the fraction of their elements assigned to the same edge community. Repeating that process for all pairs of brain regions generated a node-by-node similarity matrix (Figure 4C). Considering, separately, the within-system elements for each system, we found that visual and sensorimotor systems exhibited significantly greater levels of similarity compared with the other brain systems (permutation test, 1,000 repetitions; $p < 10^{-3}$; Figures 4D and 4E). With a similar analysis, we also found that the control network exhibited significantly lower levels of within-system similarity compared with the default mode, salience/ventral attention, somatomotor, and visual network (permutation test, 1,000 repetitions; $p < 10^{-3}$), suggesting that the edge community assignments of control-network regions are more heterogeneous relative to nodes in those other brain systems. We found similar results with different numbers of edge communities (Figure S5).

Next, we clustered the within-system similarity matrix for each system (Figure 5A). This procedure entailed extracting the set of within-system similarity values and, using a multi-scale variant of modularity maximization (Newman and Girvan, 2004), estimating clusters across a range of topological scales (by varying the value of a structural resolution parameter, γ , over the interval [0, 1] in increments of 0.002; Reichardt and Bornholdt, 2006). We then grouped together clusters estimated using similar parameter values and, from those estimates, extracted consensus clusters (Lancichinetti and Fortunato, 2012). We repeated this procedure for multiple topological scales (resolution parameters); here, we focus on the range $0.4 < \gamma < 0.5$.

In general, we found that the number of clusters detected was greatest in higher-order systems compared with somatomotor and visual networks (Figure 5B). We find similar results at other ranges of γ (see Figure S6B). Here, we focus on the control network, which the clustering algorithm partitioned into three clusters (Figure 5C; we show results for other brain systems in Figure S6A and comparisons with other reported sub-divisions in Figure S6C). Each cluster was, internally, homogeneous (Figure 5D) and composed of regions with distinct edge-community profiles (Figure 5Ee). We show these profiles in greater detail in Figures 5F-5I.

Intuitively, we can think of these profiles as delineating different patterns by which the activity of regions in the control network and the rest of the brain co-fluctuates. To map those patterns back to brain systems, we calculated the dominant edge community, linking each of the three control clusters to the eight canonical systems. We depict these cluster-to-system links as hub-and-spoke diagrams in Figures 5J-5L. At the center of each diagram is a hub that represents the set of control regions assigned to that cluster. Those regions are connected to each system by spokes colored according to the dominant edge community. For instance, edges from control regions in cluster 1 to regions belonging to the salience/ventral attention system tend to belong to the red edge community, whereas edges linking that cluster to the visual network tend to be in the cyan edge community.

Importantly, although this analysis suggests that there exist distinct modes of coordination between control regions and the rest of the brain, there were also some patterns of edge communities shared across the multiple clusters. Specifically, we found



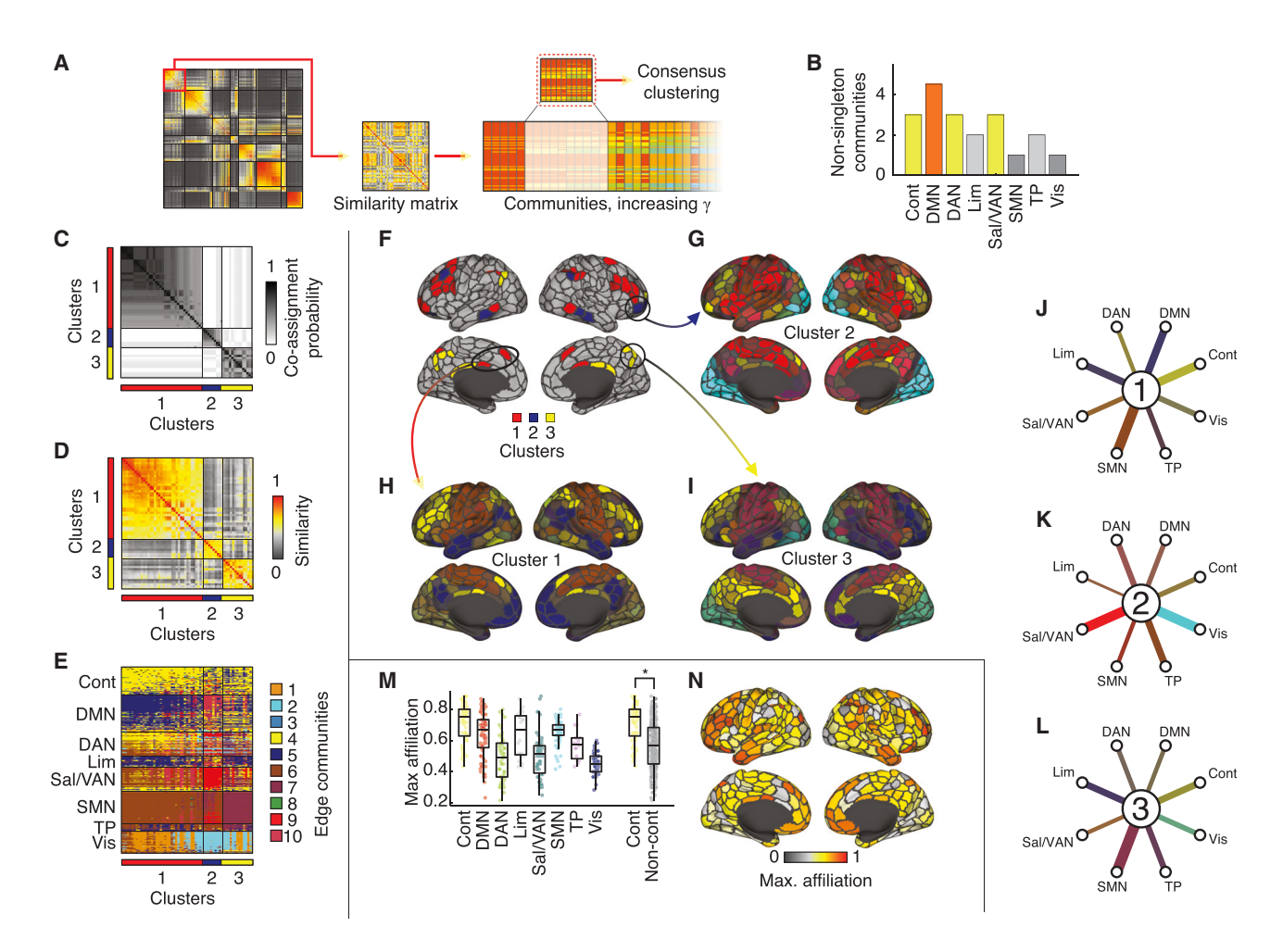


Figure 5. Cluster structure of edge communities

- (A) Pipeline for estimating system-specific multi-resolution clusters.
- (B) We found that the systems with the greatest number of communities included control, default mode, and both dorsal and ventral attention networks. In (C)–(N), we focus on the control network specifically.
- (C) Co-assignment matrix ordered by consensus communities.
- (D) The within-system similarity matrix ordered according to the three-cluster solution.
- (E) Edge community profiles ordered according to clusters.
- (F-I) Topographic representation of consensus clusters (F) and cluster centroids (G-I). In each centroid plot, nodes are colored according to the mode of their edge community assignments emanating from the control network. The brightness of nodes indicates "cluster homogeneity."
- (J-L) Hub-and-spoke plots for each centroid revealing the dominant edge community linking centroids to brain systems. In these plots, line color indicates the dominant edge community. Line thickness is linearly proportional to the fraction of connections assigned to that dominant community.
- (M and N) Maximum affiliation of control nodes to any of the 10 edge communities aggregated by brain system (M) and displayed topographically (N). In (M), asterisk indicates $p < 10^{-3}$.

that nodes in the control network tended to be linked to one another via the same edge community (Figures 5M and 5N). On the other hand, the edge community assignments of nodes in the control network to dorsal attention, salience/ventral attention, and visual networks are all highly variable. We demonstrated that statistically by partitioning nodes into control (61 regions) and non-control groups (339 regions). We calculated the average maximum affiliation over nodes in each group and calculated the difference in means (0.14). We then compared that value to a null distribution generated by permuting nodes' system labels and preserving spatial relationships. We found that the observed

difference exceeded all values in our estimated null distribution (permutation test. 1.000 repetitions: $p < 10^{-3}$).

Taken together, these findings indicate that the internal structure and complexity of edge communities varies across systems. Building on observations from the previous section, and in agreement with the extant literature, we find that the greatest level of complexity is located in the higher-order, heteromodal brain systems, which are associated with a range of cognitive domains. Our findings suggest that their polyfunctionality may be engendered by the diversity of edge-communities profiles.

Article



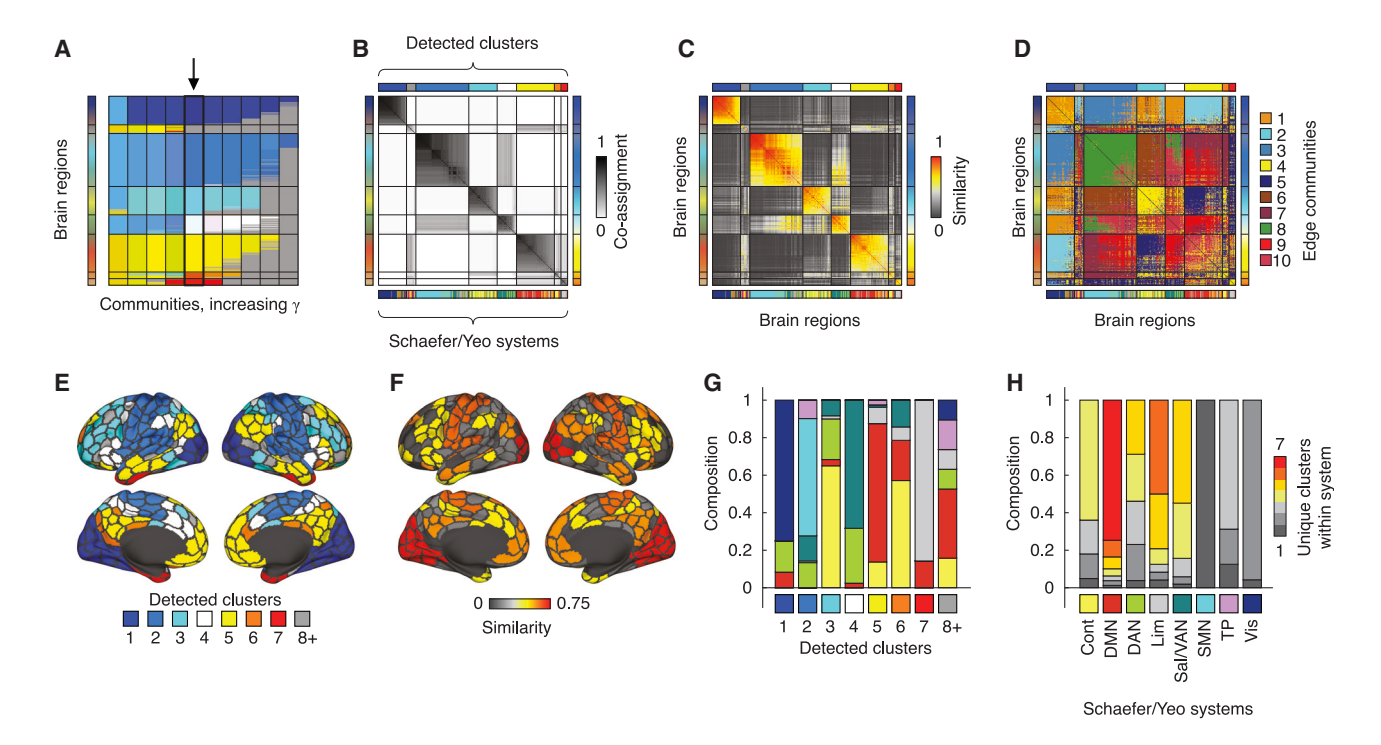


Figure 6. Multi-resolution cluster structure of cortical edge communities

(A) Nodes' cluster assignments arranged in order from coarsest to finest levels. In our analysis, we focus on a level in which there seven large clusters comprising >20 nodes each (black arrow) exist. Note that the nodes are ordered by clusters detected and not brain systems. The bar on the x axis depicts brain system labels in the same ordering.

(B-D) Interregional cluster co-assignment probabilities (B), whole-brain edge community similarities (C), and edge community labels in matrix form (D), ordered by

- (E) Clusters mapped onto the cortical surface. Small clusters are collapsed into a single label (gray).
- (F) Regional similarity of detected clusters and canonical brain systems.
- (G) System composition of detected clusters.
- (H) Cluster composition of brain systems. Color indicates the number of unique clusters within a system.

Uncovering whole-brain communities from edge community profiles

In Multi-scale and system-dependent organization, we used a multi-resolution community-detection algorithm to uncover the cluster structure of edge communities within specific brain systems. Although these analyses revealed differences from one system to another, they prevented us from discovering patterns in edge communities at the whole-brain level. For instance, if two nodes had identical edge community profiles but were assigned to different systems, the previous analyses would be incapable of grouping them together into the same cluster. To address those limitations, we used the same algorithm as in the previous section to uncover multi-scale community structure using wholebrain data. We found that clusters derived from edge communities largely approximated known cognitive systems. However, we also uncovered subtle, yet systematic, differences between nodes' assigned clusters and their canonical system labels.

We applied a multi-resolution consensus clustering algorithm to partition the cerebral cortex into non-overlapping communities of different sizes (Figure 6A). Here, we focus on an intermediate scale that resulted in seven large clusters and multiple small clusters (which we group into a separate cluster for convenience) (Figure 6B). We note that the larger clusters tended to be stable across the full range of γ values. At an intermediate level (0.4 $< \gamma <$ 0.5), nodes assigned to the detected clusters were similar to one another (Figure 6C), resulting in homogeneous edge community profiles (Figure 6D; we show partitions derived at other resolutions in Figure S7A). We also confirm that the edge communities detected using this data-driven method are more homogeneous than the brain systems analyzed in previous sections. Specifically, we separately pooled within-cluster and within-system similarity values and compared their means. As expected, we found that the within-cluster similarity values were significantly greater than the within-system values (t test; $p < 10^{-15}$; see Figure S7B).

Broadly, the detected clusters were similar to known brain systems (Figure 6E). To assess this correspondence more directly, we computed the similarity (Jaccard index) of each region's assigned cluster and system. Overall, the visual and somatomotor networks exhibited greater-than-expected similarity, whereas control, dorsal attention, limbic, and temporoparietal networks were more dissimilar than expected ($p_{adi} = 0.0016$; false discovery rate fixed at 5%; Figure 6F). To better visualize the overlap, we calculated the composition of each cluster in terms of its assigned node's system labels (Figure 6G). We found that clusters 1 and 2 were almost uniformly composed of regions



from the visual and somatomotor systems, respectively. Similarly, clusters 3, 4, 5, 6, and 7 were dominated by nodes in the control, salience/ventral attention, default mode, control, and limbic systems, respectively. Interestingly, cluster 8 (which was an aggregate of all the small communities) included relatively few sensorimotor nodes and was composed of regions from control, default mode, attention, limbic, and temporoparietal systems. We performed a similar analysis, grouping the detected clusters by brain systems (Figure 6H). We found that visual and somatomotor systems were composed of relatively few distinct clusters, whereas the other brain systems were composed of nodes from multiple different clusters. To test that statistically, we partitioned nodes into three groups: visual, somatomotor, and everything else. We computed the entropies for each group based on the distribution of nodes' cluster labels and the differences in their entropies. We then compared those differences with a null distribution generated by randomly permuting system labels and preserving spatial relationships. We found that the differences observed were significantly greater than chance, confirming that visual and somatomotor systems were composed of fewer clusters than other systems (permutation test, 1,000 repetitions; $p < 10^{-3}$).

Collectively, these results suggest that the similarity of regions' edge community profiles is largely aligned with the brain's known system-level organization. However, we also find that differences between the two sets of labels follow a distinct pattern. Misalignment tends to involve regions typically assigned to heteromodal systems.

Edge community structure is subject specific

To this point, all analyses have focused on relating brain systems to edge communities using pooled, group-representative data. These analyses uncovered shared relationships, common across a small cohort of individuals. However, there remain several important unresolved questions. For instance, to what extent are edge communities variable across individuals? Are the edge community profiles of some regions and systems differentially variable across individuals? Does variability of those features reflect meaningful, subject-specific traits? Here, we address these questions by detecting and comparing edge communities within and between subjects and scans.

To address those questions, we performed three separate analyses. First, for each subject, we concatenated their scans and estimated their subject-specific consensus edge communities (Figure 7A). Subjects' edge communities were more similar to group-representative partition than expected by chance (permutation test, 1,000 repetitions; $p < 10^{-3}$).

Visual inspection revealed that edge communities were heterogeneous across subjects, suggesting that edge communities might capture idiosyncratic and subject-specific variation. To test that hypothesis, we estimated edge communities for each subject and each scan (Figure 7B). If edge communities were unique to individual subjects, then, we would expect that imposing them on another scan from the same subject would result in segregated edge communities (strong internal eFC; weak external eFC). On the other hand, imposing those edge partitions onto eFC from a different individual would result in reduced segregation. We tested that hypothesis by systemati-

cally imposing each of the 100 edge partitions onto eFC estimated from 10 subjects and their 10 scans (100 scans in total) and calculated the "segregation" score as the mean within-community eFC minus the mean between-community eFC (Figure 7C). As expected, we found that segregation was greatest when we imposed a partition back on the eFC used to estimate those edge communities in the first place (t test; $p < 10^{-15}$; Figure 7D). Interestingly, we also found the segregation was greater when we imposed edge communities on eFC estimated from the same individual than on eFC estimated from other individuals (t test; p < 10^{-15} ; Figure 7D). These observations suggest that edge communities capture meaningful, subject-specific patterns of edge-edge interactions. Note that these analyses are similar in spirit to previous reports that the variability of individual edge-edge connections is subject specific (Faskowitz et al., 2020). The current findings focus on the variability of communities-a coarser scale of description-and indicate that the subject specificity of edge-edge connections propagates to, and manifests at, this scale.

These analyses, however, did not reveal what parts of the brain make subjects identifiable. Here, we address that question by estimating the differential identifiability associated with the edge community structure of every brain region. Specifically, for a given scan and subject, we can generate a vector-region i's similarity with respect to all $i \neq i$ (Figure 7E). Here, i indexes other regions' vectors. We can then extract analogous vectors from that subject's other scans and from all subjects' and their respective scans. Calculating the matrix of pairwise correlations, we compute the differential identifiability as the mean withinsubject similarity minus the mean between-subject similarity. We then repeat this procedure for all regions.

This procedure generates a score for every brain region that describes, on average, how personalized and idiosyncratic its edge communities are. In Figure 7F, we show those scores projected onto the cortical surface. Interestingly, we find considerable variability across the cortex in terms of identifiability, with regions in the control network, along with temporoparietal and dorsal attention networks performing particularly well (Figure 7G). We find similar results using different numbers of communities (see Figure S8).

In summary, these results further implicate the control network, along with other areas in attentional and temporoparietal networks, as key drivers of individuality in edge communities. Our work builds on a previously established quantitative framework for tracking identifiable features of brain imaging and network data (Amico and Goñi, 2018), and extends this framework using edge connectivity data. In doing so, we rely on a mapping of edge communities back into a node-centric framework, thereby improving their interpretability.

Overall, these findings suggest that edge communities are highly personalized and that this personalization can be linked to the variability of edge communities associated with many different systems in general but, in particular, the cognitive control network. These observations agree with other recent studies reporting that control networks carry personalized information about subjects (Finn et al., 2015). In summary, our findings underscore the inter-subject variability of the brain's community and system-level architecture, complementing companion

Article



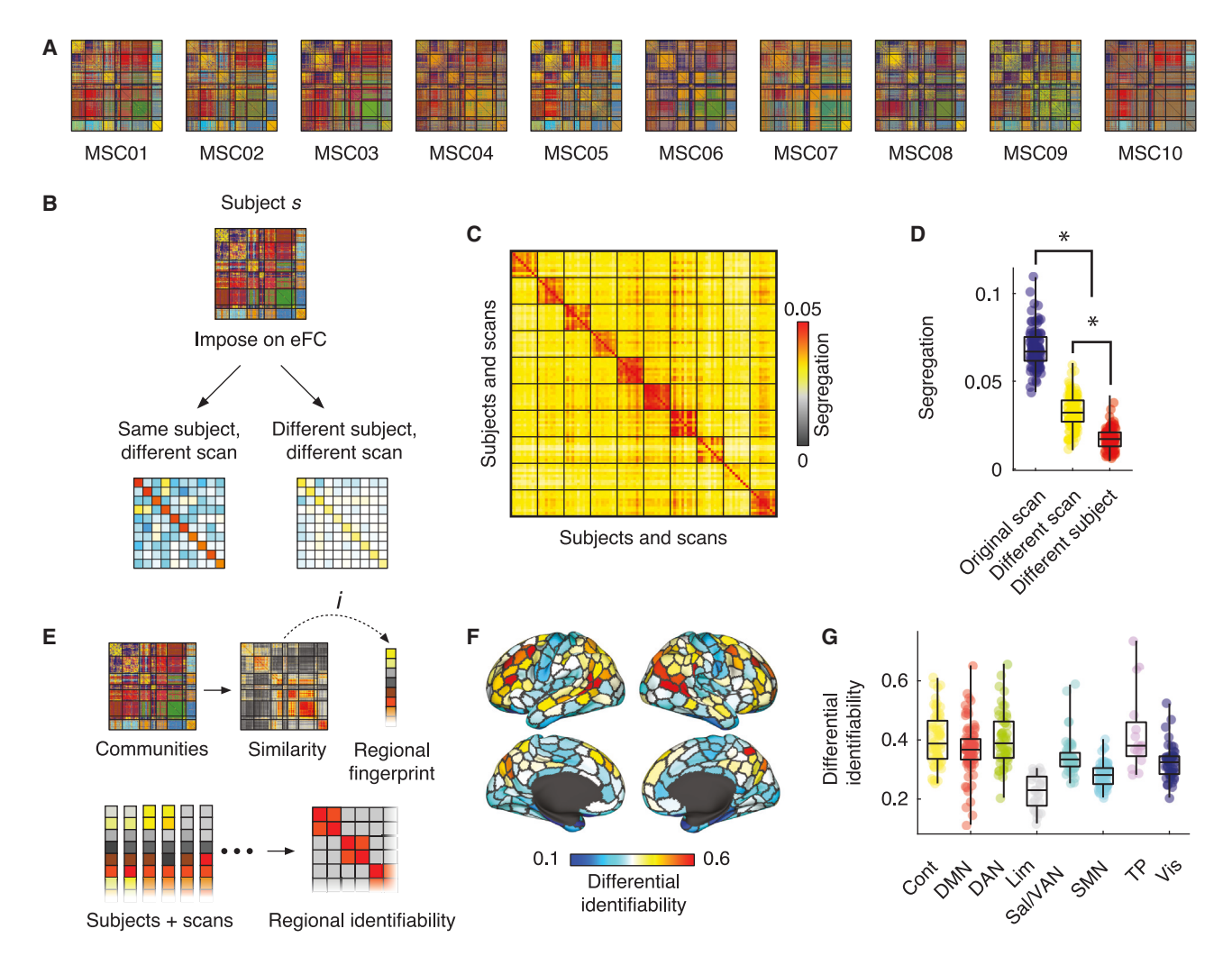


Figure 7. Personalization of edge community structure

- (A) Subject-representative edge communities (estimated with 10 scans).
- (B) Pipeline for segregation estimation. We derived edge communities for each subject and each scan and imposed those communities onto eFCs estimated from all other scans and subjects. Segregation is measured as the mean within-community eFC minus the mean between-community eFC.
- (C) Scan-by-scan matrix of segregation scores; rows represent the subject and scan from which edge communities were estimated, and columns represent the subject and scan onto which those communities were imposed. The brightness of cells represents the level of segregation.
- (D) Comparing segregation scores within and between scans/subjects. Asterisk indicates p < 10⁻¹⁵.
- (E) Pipeline for calculating regional differential identifiability.
- (F) Topographic representation of regional differential identifiability scores.
- (G) Regional differential identifiability scores aggregated by brain systems.

analyses of MSC data using node-centric models of connectivity (Gratton et al., 2018; Gordon et al., 2017b).

DISCUSSION

In this paper, we investigated the configuration of edge communities across canonical brain systems. We found that all pairs of systems were linked to one another by at least two edge communities and that the exact number and diversity of such links varied by system. Focusing only on within-system edges, we found that the variability and diversity of edge communities comprising higher-order cognitive systems was greater than that of sensorimotor systems. We then used a data-driven clustering algorithm

to partition brain regions in each brain system into multi-scale communities, according to the similarity of their edge community profiles. We found that the number of communities detected is greatest in heteromodal systems and lowest in sensorimotor systems. Repeating this analysis using data from the complete cerebral cortex, we discovered that, overall, the clusters detected resembled known brain systems. However, there were also systematic discrepancies between system labels and the clusters detected, revealing incongruity between clusters derived from traditional nFC and those derived from eFC. Finally, we show that edge community structure is subject specific and reproducible across multiple scans of the same individual. This personalization is driven by the edge community assignments





of nodes located in control, default mode, dorsal attention, and temporoparietal networks.

Pervasive overlap and multiplexity

Many studies have partitioned brain regions based on their functional connections, revealing a surprisingly consistent set of communities that align well with activation patterns and wellknown brain systems (Power et al., 2011; Thomas Yeo et al., 2011; Meunier et al., 2009; Sporns and Betzel, 2016). These observations suggest that assortative and segregated communities may play an important role in the emergence of functional specialization. Here, rather than focus on partitions of brain regions into communities, we leveraged a recently proposed edge-centric network model to partition connections into communities (Zamani Esfahlani et al., 2020b; Faskowitz et al., 2020). The resulting edge communities delineate groups of functional connections whose valence and amplitude co-fluctuate with one another over time. We speculate that these co-fluctuation patterns may correspond to distinct modes of interregional communication.

A key question, then, was whether edge communities were aligned with the boundaries of traditionally defined brain systems. That is, if we were to examine the complete set of connections between regions in systems A and B, would those connections co-fluctuate uniformly and be assigned to a single edge community, or would they be composed of several distinct patterns of co-fluctuation? Phrased alternatively, and in line with the hypothesis that co-fluctuating edges reflect distinct modes of interregional communication, do systems communicate with one another through a single homogeneous mode or do they communicate in parallel via a series of multiplexed channels? Here, we addressed that question by counting the number and distribution of edge communities linking pairs of systems. In all cases, systems were linked by multiple edge communities, although the number and diversity varied considerably across system pairs. These observations suggest that the brain exists in a state of "pervasive overlap" (Ahn et al., 2010; Faskowitz et al., 2020), in which regions and systems throughout the brain are linked to one another through multiple edge communities.

Our findings have important implications for understanding brain function. In most studies, brain regions are assigned to non-overlapping communities with distinct functional profiles (Power et al., 2011; Gordon et al., 2016; Thomas Yeo et al., 2011). Polyfunctionality emerges from this caricature in the form of a small subset of brain regions whose connectivity patterns span system boundaries (Bertolero et al., 2015, 2017). On the other hand, we find that all brain regions participate in many communities and the functional connections bridging brain systems are associated with a plurality set of community labels. These observations suggest that overlapping function may be a key organizing principle of brain networks and a rule, rather than an exception.

Why, then, do we observe multiplexed, overlapping community structure in the brain? Why are the same brain systems linked by dissimilar patterns of co-fluctuation? One obvious possibility is that the current system ontology does not fully capture the sub-divisions and fine-scale structure of cortical architecture (Uddin et al., 2019). That is, edge communities may reveal orga-

nization that is obscured by, or inaccessible, using node-centric network models. Another possibility is that edge communities reflect a form of functional robustness and redundancy (Pessoa, 2014). That is, by communicating across multiple "channels," brain systems reduce the likelihood that damage to any one channel would result in a complete disruption of communication and brain function (Aerts et al., 2016; Betzel and Bassett, 2018; Honey and Sporns, 2008; Alstott et al., 2009). Future work is necessary to clarify the precise functional roles of multiplexed and overlapping communities.

Heterogeneity and system specificity of edge community profiles

Here, we examined edge communities from the perspective of brain regions by defining edge community "profiles." Focusing on profiles, we were able to map edge communities from an unfamiliar and large *m*-dimensional edge space back into an *n*-dimensional node space. By studying the similarity of regions' profiles to one another, we were able to characterize the diversity of edge communities among regions that make up traditional brain systems. Using that approach, we generated region-by-region similarity matrices for every system and clustered them using a multi-resolution algorithm.

Interestingly, the internal structure of edge community profiles varied across brain systems, with the regions in sensorimotor systems exhibiting highly similar edge community profiles and regions in higher order, heteromodal systems exhibiting greater variation. These observations agree with current theories of cortical organization and function. In terms of node-centric community structure, sensorimotor systems are among the most functionally segregated (Power et al., 2011, 2013) and occupy opposite positions along smoothly varying functional gradients (Margulies et al., 2016).

The same analysis pipeline was applied to similarity matrices constructed using edge community profiles from the entire cerebral cortex. Specifically, the communities detected resembled known system-level divisions of cortex (Schaefer et al., 2017). We found that regions associated with higher-order brain systems were more likely to fragment and form small (sometimes singleton) clusters with distinct edge community profiles. Importantly, the detected clusters were inhomogeneous and contained regions associated with multiple brain systems. Collectively, these findings suggest that edge communities give rise to distinct regional profiles that are organized into clusters that span traditional system-level boundaries.

Personalization of edge community structure

Most of this report focused on edge community structure using composite edge time series assembled from multiple subjects. Although analysis of group-representative data can uncover patterns of eFC shared across many individuals, it is poorly suited for uncovering personalized and idiosyncratic features of eFC, which are key elements necessary for biomarker generation (Woo and Wager, 2015; Wang et al., 2020). Addressing this limitation, we derived edge communities for the ten individuals in the MSC dataset. We found that subjects' edge community structure was idiosyncratic, so communities estimated from subject s using data from scan t did a good job describing

Article



edge communities of the same subject on scan t' but a poor job describing edge communities of any other subject. Importantly, these idiosyncrasies arise from the community assignments of edges associated with control, default mode, dorsal attention, and temporoparietal networks.

These observations agree with other recent analysis of MSC data, reporting high levels of personalization in both cortical and subcortical networks (Gratton et al., 2018; Sylvester et al., 2020; Gordon et al., 2017b, 2018). Like similar findings in larger populations (Finn et al., 2015; Amico and Goñi, 2018) our findings implicate heteromodal association cortex as being both highly repeatable across scans of the same subject but maximally dissimilar across individuals. These observations suggest that edge communities, which we interpret as modes of temporally resolved accounts of ongoing communication between brain regions, are also subject specific and personalized. We further link the personalization of edge community structure to the assignments of edges associated with higher-order cognitive systems, including control, default mode, dorsal attention, and temporoparietal networks. The findings reported here align with other recent studies suggesting brain network organization is highly individualized (Gratton et al., 2018, 2019; Sylvester et al., 2020; Gordon et al., 2017b; Seitzman et al., 2019; Cui et al., 2020). Collectively, these observations open up the tantalizing prospect of more targeted and increasingly personalized interventions in the future.

Future directions

Our work opens up several opportunities for future studies, both methodological and applied. For instance, are inter-individual differences in the number and diversity of edge communities between brain systems related to behavioral, demographic, and clinical variables of interest, such as a subject's performance on a cognitively demanding task (Shirer et al., 2012), their biological age (Zuo et al., 2017), or their neuropsychiatric state (Fornito et al., 2015)? Similarly, future studies should investigate individual differences in the composition and sub-divisions of brain systems. For example, is the complexity and heterogeneity of edge community profiles within subjects' control networks related to their performance on tasks that require cognitive control, e.g., Stroop or Navon tasks (Medaglia et al., 2018; Betzel et al., 2018b)?

Other potentially fruitful opportunities for future studies include exploring subcortical (Sylvester et al., 2020) and cerebellar organization (King et al., 2019) with edge communities. These areas were excluded from the present study but could be investigated in greater detail, yielding new insight into cortical-subcortical interactions (Ji et al., 2019). Relatedly, features derived from edgecentric network models, including overlapping communities, could be incorporated into parcellation-generation frameworks to create novel cortical parcellations (Eickhoff et al., 2018).

A final direction for future research involves exploring the relative utility of edge time series and eFC compared with more traditional constructs, such as sliding window estimates of time-varying connectivity and nFC. Compared with sliding window estimates, edge time series require no parameterization and do not necessitate a sliding window, making it possible to track framewise estimates of edge weights. Similarly, eFC can be used to detect pervasively overlapping communities, yielding new

insight into the brain's modular structure (Faskowitz et al., 2020). Although recent work suggests that these and other features of edge-centric analyses can be exploited to learn more about brain organization and dynamics, few studies have systematically compared them with more common methods (Zamani Esfahlani et al., 2021a; Novelli and Razi, 2021). Future work should investigate these questions in greater detail.

Limitations of the study

One overarching limitation surrounding this study concerns the interpretability of eFC. Although traditional nFC is now largely accepted within the human neuroimaging community and is frequently interpreted as a measure of interregional communication (although with many caveats; Reid et al., 2019), eFC is novel, high dimensional, and may be difficult to interpret. Although this study attempts to form a conceptual bridge between the systemlevel organization of nFC and edge communities, future work is necessary to clarify, in more precise terms, the relationship between these two constructs.

A second limitation concerns the procedure for estimating edge communities. Here, we use a k-means algorithm that partitions edges into a fixed number of clusters on the basis of their similarity (eFC) with respect to one another. The motivation to use k-means as opposed to other clustering algorithms was practical and stems from its computational efficiency and the fact that eFC can be viewed as a distance metric and can be used by the k-means algorithm to estimate edge communities from edge time series directly. However, there exists a multitude of alternative algorithms that could, in principle, be applied to edge time series or eFC to estimate communities, including the suite of graph-clustering algorithms (Fortunato, 2010; Porter et al., 2009) but also time-series decompositions algorithms, such as independent components analysis (ICA) (Hyvärinen and Oja, 2000), which has proven especially useful in the analysis of neuroimaging data (Beckmann et al., 2005). Applying many of these algorithms to eFC data, however, would require computing, storing, and manipulating massive, fully weighted, and signed matrices. For large, multi-subject datasets this presents an undesirable computational burden. Along with investigating the effect of clustering algorithms, future studies should also explore solutions that also help reduce the computational burden of discovering edge communities.

Here, we use a recently proposed framework to transform node-centric fMRI data into edge-centric networks (Zamani Esfahlani et al., 2020b; Faskowitz et al., 2020). This framework complements extant approaches that aim to do the same. These include line graphs (Evans and Lambiotte, 2009) and link similarity (Ahn et al., 2010), as well as non-linear embedding techniques (Gao et al., 2020). Although, in principle, these methods all achieve the same goal of generating edge-centric networks, they achieve this through different means, possess distinct biases, and likely, yield complementary insight into the edgelevel organization of networks. Indeed, early results suggest that this is the case. In Faskowitz et al. (2020), for instance, the authors compare the community structure obtained by clustering line graphs and eFC matrices. In general, the patterns are dissimilar, suggesting that these two approaches capture distinct edge-level features of a network.





Moving forward, an increasingly important line of work will be the construction of appropriate null models for eFC. For all the above-mentioned methods, it is critical that the null models be implemented at the nodal level. Recent studies have shown that at least some of the properties of edge-centric networks are mathematical necessities that arise from the network construction process and can be, in part, anticipated from the node-level networks directly (Novelli and Razi, 2021). A null model implemented at the level of edge networks may fail to preserve those properties. In the case of eFC, the appropriate null model likely operates directly on the nodal time series. Among the possible candidates are multivariate autoregressive models (Liégeois et al., 2017) or phase randomized surrogates (Zalesky et al., 2014). At present, however, there is a lack of consensus as to what the appropriate null model should be, with some studies using generating null time series based on circular shifts of the original data (Greenwell et al., 2021; Betzel et al., 2021), whereas others explore complex biophysical models (Pope et al., 2021). In summary, future work should explore both the effect of the method for generating edge-centric networks as well as the utility of different null models for identifying statistically meaningful features of those networks.

A final limitation concerns the eFC measure itself. In general, eFC assesses the similarity of edge time series originating from two pairs of nodes, $\{i, j\}$ and $\{u, v\}$. In most cases, $i \neq u \neq v$. However, some node pairs may share a node, that is, either i or j is equal to either u or v. The presence of a shared node may inflate the similarity of their edge time series, yielding spuriously strong eFC weights. Here, we do not correct for that possibility explicitly because it falls beyond the scope of our study. However, future studies should explore strategies for mitigating the possibility of spurious eFC. One possibility is to perform careful comparisons of observed eFC with eFC estimated from time-series surrogates. If the observed eFC is artifactually inflated because of shared nodes, we expect to find similar inflation in the surrogate data, which can then be subtracted or modeled out of the observed eFC. Another possibility is to censor edge-edge connections that involve a shared node, that is, impute those elements in the eFC matrix with a value of 0 or as NaN, effectively nullifying their contribution to all subsequent analyses.

Conclusion

In summary, detailed analysis of edge functional connectivity and edge communities revealed marked heterogeneity across brain systems and highly reproducible and idiosyncratic patterns within subjects. These findings help establish edge functional connectivity as a useful representational framework and edge communities as measures of potential interest for revealing novel brain-behavior associations and individual differences in brain organization.

STAR*METHODS

Detailed methods are provided in the online version of this paper and include the following:

- KEY RESOURCES TABLE
- RESOURCE AVAILABILITY

- Lead contact
- Material availability
- Data and code availability
- EXPERIMENTAL MODEL AND SUBJECT DETAILS
- METHOD DETAILS
 - Functional preprocessing
 - Image quality control
- QUANTIFICATION AND STATISTICAL ANALYSIS
 - Parcellation preprocessing
 - Functional network preprocessing
 - Edge graph construction
 - O Edge community detection algorithm
 - Community overlap metrics
 - Edge community similarity
 - Modularity maximization
 - Edge community segregation
 - Differential identifiability

SUPPLEMENTAL INFORMATION

Supplemental information can be found online at https://doi.org/10.1016/j.ceirep.2021.110032.

ACKNOWLEDGMENTS

This material is based upon work supported by the National Science Foundation under grant no. 076059-00003C (R.F.B. and O.S.). This research was supported by Indiana University Office of the Vice President for Research Emerging Area of Research Initiative, Learning: Brains, Machines and Children (F.Z.E., O.S., and R.F.B.).

AUTHOR CONTRIBUTIONS

Y.J. and R.F.B. conceived of the project, performed analyses, and wrote the initial draft of the manuscript. J.F. processed imaging data. All authors edited manuscript and contributed to final version.

DECLARATION OF INTERESTS

The authors declare no competing interests.

Received: July 24, 2021 Revised: September 8, 2021 Accepted: October 28, 2021 Published: November 16, 2021

REFERENCES

Abraham, A., Pedregosa, F., Eickenberg, M., Gervais, P., Mueller, A., Kossaifi, J., Gramfort, A., Thirion, B., and Varoquaux, G. (2014). Machine learning for neuroimaging with scikit-learn. Front. Neuroinform. 8, 14.

Aerts, H., Fias, W., Caeyenberghs, K., and Marinazzo, D. (2016). Brain networks under attack: robustness properties and the impact of lesions. Brain 139, 3063–3083.

Ahn, Y.-Y., Bagrow, J.P., and Lehmann, S. (2010). Link communities reveal multiscale complexity in networks. Nature *466*, 761–764.

Alstott, J., Breakspear, M., Hagmann, P., Cammoun, L., and Sporns, O. (2009). Modeling the impact of lesions in the human brain. PLoS Comput. Biol. 5, e1000408.

Amico, E., and Goñi, J. (2018). The quest for identifiability in human functional connectomes. Sci. Rep. 8, 8254.

Article



Avants, B.B., Epstein, C.L., Grossman, M., and Gee, J.C. (2008). Symmetric diffeomorphic image registration with cross-correlation: evaluating automated labeling of elderly and neurodegenerative brain. Med. Image Anal. 12, 26-41.

Avants, B.B., Tustison, N., Song, G., et al. (2009). Advanced normalization tools (ants). Insight J. 2, 1-35.

Bassett, D.S., and Sporns, O. (2017). Network neuroscience. Nat. Neurosci. 20, 353-364.

Bassett, D.S., Greenfield, D.L., Meyer-Lindenberg, A., Weinberger, D.R., Moore, S.W., and Bullmore, E.T. (2010). Efficient physical embedding of topologically complex information processing networks in brains and computer circuits. PLoS Comput. Biol. 6, e1000748.

Bassett, D.S., Porter, M.A., Wymbs, N.F., Grafton, S.T., Carlson, J.M., and Mucha, P.J. (2013). Robust detection of dynamic community structure in networks. Chaos 23, 013142.

Bazzi, M., Porter, M.A., Williams, S., McDonald, M., Fenn, D.J., and Howison, S.D. (2016). Community detection in temporal multilayer networks, with an application to correlation networks. Multiscale Model. Simul. 14, 1-41.

Beckmann, C.F., DeLuca, M., Devlin, J.T., and Smith, S.M. (2005). Investigations into resting-state connectivity using independent component analysis. Philos. Trans. R. Soc. Lond. B Biol. Sci. 360, 1001-1013.

Bertolero, M.A., Thomas Yeo, B.T., and D'Esposito, M. (2015). The modular and integrative functional architecture of the human brain. Proc. Natl. Acad. Sci. USA 112, E6798-E6807.

Bertolero, M.A., Thomas Yeo, B.T., and D'Esposito, M. (2017). The diverse club. Nat. Commun. 8, 1277.

Betzel, R. (2018). Organizing principles of whole-brain functional connectivity in zebrafish larvae. bioRxiv, 496414.

Betzel, R.F. (2020). Community detection in network neuroscience. arXiv, ar-Xiv:2011.06723v1.

Betzel, R.F., and Bassett, D.S. (2017). Multi-scale brain networks. Neuroimage 160, 73-83.

Betzel, R.F., and Bassett, D.S. (2018). Specificity and robustness of long-distance connections in weighted, interareal connectomes. Proc. Natl. Acad. Sci. USA 115. E4880-E4889.

Betzel, R.F., Medaglia, J.D., Papadopoulos, L., Baum, G.L., Gur, R., Gur, R., Roalf, D., Satterthwaite, T.D., and Bassett, D.S. (2017). The modular organization of human anatomical brain networks: Accounting for the cost of wiring. Netw. Neurosci. 1, 42-68.

Betzel, R.F., Bertolero, M.A., and Bassett, D.S. (2018a). Non-assortative community structure in resting and task-evoked functional brain networks. bioRxiv, 355016.

Betzel, R.F., Medaglia, J.D., and Bassett, D.S. (2018b). Diversity of meso-scale architecture in human and non-human connectomes. Nat. Commun. 9, 346.

Betzel, R.F., Bertolero, M.A., Gordon, E.M., Gratton, C., Dosenbach, N.U.F., and Bassett, D.S. (2019a). The community structure of functional brain networks exhibits scale-specific patterns of inter- and intra-subject variability. Neuroimage 202, 115990.

Betzel, R., Cutts, S., Greenwell, S., and Sporns, O. (2021). Individualized event structure drives individual differences in whole-brain functional connectivity. bioRxiv. https://doi.org/10.1101/2021.03.12.435168.

Betzel, R.F., Medaglia, J.D., Kahn, A.E., Soffer, J., Schonhaut, D.R., and Bassett, D.S. (2019b). Structural, geometric and genetic factors predict interregional brain connectivity patterns probed by electrocorticography. Nat. Biomed. Eng. 3, 902-916.

Blondel, V.D., Guillaume, J.-L., Lambiotte, R., and Lefebvre, E. (2008). Fast unfolding of communities in large networks. J. Stat. Mech. (10), P10008.

Bullmore, E., and Sporns, O. (2009). Complex brain networks: graph theoretical analysis of structural and functional systems. Nat. Rev. Neurosci. 10, 186-198.

Cox, R.W. (1996). AFNI: Software for analysis and visualization of functional magnetic resonance neuroimages. Comput. Biomed. Res. 29, 162-173.

Craddock, R.C., Jbabdi, S., Yan, C.-G., Vogelstein, J.T., Castellanos, F.X., Di Martino, A., Kelly, C., Heberlein, K., Colcombe, S., and Milham, M.P. (2013). Imaging human connectomes at the macroscale. Nat. Methods 10, 524–539.

Cui, Z., Li, H., Xia, C.H., Larsen, B., Adebimpe, A., Baum, G.L., Cieslak, M., Gur, R.E., Gur, R.C., Moore, T.M., et al. (2020). Individual variation in functional topography of association networks in youth. Neuron 106, 340-353.e8.

Dale, A.M., Fischl, B., and Sereno, M.I. (1999). Cortical surface-based analysis. I. Segmentation and surface reconstruction. Neuroimage 9, 179–194.

De Domenico, M. (2017). Multilayer modeling and analysis of human brain networks. Gigascience 6, 1-8.

Di Martino, A., Fair, D.A., Kelly, C., Satterthwaite, T.D., Castellanos, F.X., Thomason, M.E., Craddock, R.C., Luna, B., Leventhal, B.L., Zuo, X.-N., and Milham, M.P. (2014). Unraveling the miswired connectome: a developmental perspective. Neuron 83, 1335-1353.

Eickhoff, S.B., Thomas Yeo, B.T., and Genon, S. (2018). Imaging-based parcellations of the human brain. Nat. Rev. Neurosci. 19, 672-686.

Esteban, O., Birman, D., Schaer, M., Koyejo, O.O., Poldrack, R.A., and Gorgolewski, K.J. (2017). MRIQC: Advancing the automatic prediction of image quality in MRI from unseen sites. PLoS ONE 12, e0184661.

Esteban, O., Markiewicz, C., Blair, R.W., Moodie, C., Isik, A.I., Erramuzpe Aliaga, A., Kent, J., Goncalves, M., DuPre, E., Snyder, M., et al. (2018). fMRI-Prep: A robust preprocessing pipeline for functional MRI. Nat. Methods 16,

Evans, T.S., and Lambiotte, R. (2009). Line graphs, link partitions, and overlapping communities. Phys. Rev. E Stat. Nonlin. Soft Matter Phys. 80, 016105.

Faskowitz, J., Yan, X., Zuo, X.-N., and Sporns, O. (2018). Weighted stochastic block models of the human connectome across the life span. Sci. Rep. 8, 12997.

Faskowitz, J., Esfahlani, F.Z., Jo, Y., Sporns, O., and Betzel, R.F. (2020). Edgecentric functional network representations of human cerebral cortex reveal overlapping system-level architecture. Nat. Neurosci. 23, 1644-1654.

Finn, E.S., Shen, X., Scheinost, D., Rosenberg, M.D., Huang, J., Chun, M.M., Papademetris, X., and Constable, R.T. (2015). Functional connectome fingerprinting: Identifying individuals using patterns of brain connectivity. Nat. Neurosci. 18. 1664-1671.

Fischl, B., van der Kouwe, A., Destrieux, C., Halgren, E., Ségonne, F., Salat, D.H., Busa, E., Seidman, L.J., Goldstein, J., Kennedy, D., et al. (2004). Automatically parcellating the human cerebral cortex. Cereb. Cortex 14, 11-22.

Fonov, V., Evans, A., McKinstry, R., Almli, C., and Collins, D. (2009). Unbiased nonlinear average age-appropriate brain templates from birth to adulthood. Neuroimage 47 (Suppl 1), S102.

Fornito, A., Zalesky, A., and Breakspear, M. (2015). The connectomics of brain disorders. Nat. Rev. Neurosci. 16, 159-172.

Fortunato, S. (2010). Community detection in graphs. Phys. Rep. 486, 75–174. Friston, K.J., Frith, C.D., Liddle, P.F., and Frackowiak, R.S. (1993), Functional connectivity: the principal-component analysis of large (PET) data sets. J. Cereb. Blood Flow Metab. 13, 5-14.

Gao, S., Mishne, G., and Scheinost, D. (2020). Poincaré embedding reveals edge-based functional networks of the brain. In International Conference on Medical Image Computing and Computer-Assisted Intervention, A.L. Martel, P. Abolmaesumi, D. Stoyanov, D. Mateus, M.A. Zuluaga, S.K. Zhou, D. Racoceanu, and L. Joskowicz, eds. (Springer), pp. 448-457.

Gordon, E.M., Laumann, T.O., Adeyemo, B., Huckins, J.F., Kelley, W.M., and Petersen, S.E. (2016). Generation and evaluation of a cortical area parcellation from resting-state correlations. Cereb. Cortex 26, 288-303.

Gordon, E.M., Laumann, T.O., Adeyemo, B., and Petersen, S.E. (2017a). Individual variability of the system-level organization of the human brain. Cereb. Cortex 27, 386-399.

Gordon, E.M., Laumann, T.O., Gilmore, A.W., Newbold, D.J., Greene, D.J., Berg, J.J., Ortega, M., Hoyt-Drazen, C., Gratton, C., Sun, H., et al. (2017b). Precision functional mapping of individual human brains. Neuron 95, 791-807.e7.



Gordon, E.M., Lynch, C.J., Gratton, C., Laumann, T.O., Gilmore, A.W., Greene, D.J., Ortega, M., Nguyen, A.L., Schlaggar, B.L., Petersen, S.E., et al. (2018). Three distinct sets of connector hubs integrate human brain function. Cell Rep. 24, 1687-1695.e4.

Gorgolewski, K., Burns, C.D., Madison, C., Clark, D., Halchenko, Y.O., Waskom, M.L., and Ghosh, S.S. (2011). Nipype: A flexible, lightweight and extensible neuroimaging data processing framework in python. Front. Neuroinform. 5. 13.

Gratton, C., Laumann, T.O., Nielsen, A.N., Greene, D.J., Gordon, E.M., Gilmore, A.W., Nelson, S.M., Coalson, R.S., Snyder, A.Z., Schlaggar, B.L., et al. (2018). Functional brain networks are dominated by stable group and individual factors, not cognitive or daily variation. Neuron 98, 439-452.e5.

Gratton, C., Kraus, B.T., Greene, D.J., Gordon, E.M., Laumann, T.O., Nelson, S.M., Dosenbach, N.U., and Petersen, S.E. (2019). Defining individual-specific functional neuroanatomy for precision psychiatry. Biol. Psychiatry 88, 28-39.

Greenwell, S., Faskowitz, J., Pritschet, L., Santander, T., Jacobs, E.G., and Betzel, R.F. (2021). High-amplitude network co-fluctuations linked to variation in hormone concentrations over menstrual cycle. bioRxiv. https://doi.org/10. 1101/2021.07.29.453892.

Greve, D.N., and Fischl, B. (2009). Accurate and robust brain image alignment using boundary-based registration. Neuroimage 48, 63-72.

Hizanidis, J., Kouvaris, N.E., Zamora-López, G., Díaz-Guilera, A., and Antonopoulos, C.G. (2016). Chimera-like states in modular neural networks. Sci. Rep. 6. 19845.

Honey, C.J., and Sporns, O. (2008). Dynamical consequences of lesions in cortical networks. Hum. Brain Mapp. 29, 802-809.

Hyvärinen, A., and Oja, E. (2000). Independent component analysis: Algorithms and applications. Neural Netw. 13, 411-430.

Jenkinson, M., Bannister, P., Brady, M., and Smith, S. (2002). Improved optimization for the robust and accurate linear registration and motion correction of brain images. Neuroimage 17, 825-841.

Ji, J.L., Spronk, M., Kulkarni, K., Repovš, G., Anticevic, A., and Cole, M.W. (2019). Mapping the human brain's cortical-subcortical functional network organization. Neuroimage 185, 35-57.

Jutla, I.S., Jeub, L.G., and Mucha, P.J. (2011). A generalized louvain method for community detection implemented in MATLAB.

Kashtan, N., and Alon, U. (2005). Spontaneous evolution of modularity and network motifs. Proc. Natl. Acad. Sci. USA 102, 13773-13778.

Kenett, Y.N., Betzel, R.F., and Beaty, R.E. (2020). Community structure of the creative brain at rest. Neuroimage 210, 116578.

King, M., Hernandez-Castillo, C.R., Poldrack, R.A., Ivry, R.B., and Diedrichsen, J. (2019). Functional boundaries in the human cerebellum revealed by a multidomain task battery. Nat. Neurosci. 22, 1371-1378.

Kirschner, M., and Gerhart, J. (1998). Evolvability. Proc. Natl. Acad. Sci. USA 95, 8420-8427.

Klein, A., Ghosh, S.S., Bao, F.S., Giard, J., Häme, Y., Stavsky, E., Lee, N., Rossa, B., Reuter, M., Chaibub Neto, E., and Keshavan, A. (2017). Mindboggling morphometry of human brains. PLoS Comput. Biol. 13, e1005350.

Lancichinetti, A., and Fortunato, S. (2012). Consensus clustering in complex networks. Sci. Rep. 2, 336.

Liégeois, R., Laumann, T.O., Snyder, A.Z., Zhou, J., and Thomas Yeo, B.T. (2017). Interpreting temporal fluctuations in resting-state functional connectivity MRI. Neuroimage 163, 437-455.

Lindquist, M.A., Geuter, S., Wager, T.D., and Caffo, B.S. (2019). Modular preprocessing pipelines can reintroduce artifacts into fMRI data. Hum. Brain Mapp. 40, 2358-2376.

Margulies, D.S., Ghosh, S.S., Goulas, A., Falkiewicz, M., Huntenburg, J.M., Langs, G., Bezgin, G., Eickhoff, S.B., Castellanos, F.X., Petrides, M., et al. (2016). Situating the default-mode network along a principal gradient of macroscale cortical organization. Proc. Natl. Acad. Sci. USA 113, 12574-12579.

Medaglia, J.D., Huang, W., Karuza, E.A., Kelkar, A., Thompson-Schill, S.L., Ribeiro, A., and Bassett, D.S. (2018). Functional alignment with anatomical networks is associated with cognitive flexibility. Nat. Hum. Behav. 2, 156-164.

Meunier, D., Lambiotte, R., Fornito, A., Ersche, K.D., and Bullmore, E.T. (2009). Hierarchical modularity in human brain functional networks. Front. Neuroinform, 3, 37,

Meunier, D., Lambiotte, R., and Bullmore, E.T. (2010). Modular and hierarchically modular organization of brain networks. Front. Neurosci. 4, 200.

Najafi, M., McMenamin, B.W., Simon, J.Z., and Pessoa, L. (2016). Overlapping communities reveal rich structure in large-scale brain networks during rest and task conditions. Neuroimage 135, 92-106.

Newman, M.E., and Girvan, M. (2004). Finding and evaluating community structure in networks. Phys. Rev. E Stat. Nonlin. Soft Matter Phys. 69, 026113.

Novelli, L., and Razi, A. (2021). A mathematical perspective on edge-centric functional connectivity. arXiv, arXiv:2106.10631v1.

Park, H.-J., and Friston, K. (2013). Structural and functional brain networks: from connections to cognition. Science 342, 1238411.

Parkes, L., Fulcher, B., Yücel, M., and Fornito, A. (2018). An evaluation of the efficacy, reliability, and sensitivity of motion correction strategies for restingstate functional MRI. Neuroimage 171, 415-436.

Pessoa, L. (2014). Understanding brain networks and brain organization. Phys. Life Rev. 11, 400-435.

Pope, M., Fukushima, M., Betzel, R., and Sporns, O. (2021). Modular origins of high-amplitude co-fluctuations in fine-scale functional connectivity dynamics.

Porter, M.A., Onnela, J.-P., and Mucha, P.J. (2009). Communities in networks. North Am. Math. Soc. 56, 1082-1097.

Power, J.D., Cohen, A.L., Nelson, S.M., Wig, G.S., Barnes, K.A., Church, J.A., Vogel, A.C., Laumann, T.O., Miezin, F.M., Schlaggar, B.L., and Petersen, S.E. (2011). Functional network organization of the human brain. Neuron 72, 665-678.

Power, J.D., Schlaggar, B.L., Lessov-Schlaggar, C.N., and Petersen, S.E. (2013). Evidence for hubs in human functional brain networks. Neuron 79, 798-813.

Power, J.D., Mitra, A., Laumann, T.O., Snyder, A.Z., Schlaggar, B.L., and Petersen, S.E. (2014). Methods to detect, characterize, and remove motion artifact in resting state fMRI. Neuroimage 84 (Suppl C), 320-341.

Reichardt, J., and Bornholdt, S. (2006). Statistical mechanics of community detection. Phys. Rev. E Stat. Nonlin. Soft Matter Phys. 74, 016110.

Reid, A.T., Headley, D.B., Mill, R.D., Sanchez-Romero, R., Uddin, L.Q., Marinazzo, D., Lurie, D.J., Valdés-Sosa, P.A., Hanson, S.J., Biswal, B.B., et al. (2019). Advancing functional connectivity research from association to causation. Nat. Neurosci. 22, 1751-1760.

Rogers, B.P., Morgan, V.L., Newton, A.T., and Gore, J.C. (2007). Assessing functional connectivity in the human brain by fMRI. Magn. Reson. Imaging 25, 1347-1357.

Rosvall, M., and Bergstrom, C.T. (2008). Maps of random walks on complex networks reveal community structure. Proc. Natl. Acad. Sci. USA 105, 1118-

Rubinov, M., and Sporns, O. (2010). Complex network measures of brain connectivity: uses and interpretations. Neuroimage 52, 1059-1069.

Satterthwaite, T.D., Elliott, M.A., Gerraty, R.T., Ruparel, K., Loughead, J., Calkins, M.E., Eickhoff, S.B., Hakonarson, H., Gur, R.C., Gur, R.E., and Wolf, D.H. (2013). An improved framework for confound regression and filtering for control of motion artifact in the preprocessing of resting-state functional connectivity data. Neuroimage 64, 240-256.

Schaefer, A., Kong, R., Gordon, E.M., Laumann, T.O., Zuo, X.-N., Holmes, A.J., Eickhoff, S.B., and Thomas Yeo, B.T. (2018). Local-global parcellation of the human cerebral cortex from intrinsic functional connectivity mri. Cereb. Cortex 28, 3095-3114.

Seitzman, B.A., Gratton, C., Laumann, T.O., Gordon, E.M., Adeyemo, B., Dworetsky, A., Kraus, B.T., Gilmore, A.W., Berg, J.J., Ortega, M., et al.

Article



(2019). Trait-like variants in human functional brain networks. Proc. Natl. Acad. Sci. USA 116, 22851-22861.

Shirer, W.R., Ryali, S., Rykhlevskaia, E., Menon, V., and Greicius, M.D. (2012). Decoding subject-driven cognitive states with whole-brain connectivity patterns. Cereb. Cortex 22, 158-165.

Smith, S.M., Jenkinson, M., Woolrich, M.W., Beckmann, C.F., Behrens, T.E., Johansen-Berg, H., Bannister, P.R., De Luca, M., Drobnjak, I., Flitney, D.E., et al. (2004). Advances in functional and structural MR image analysis and implementation as FSL. Neuroimage 23 (Suppl 1), S208-S219.

Smith, S.M., Fox, P.T., Miller, K.L., Glahn, D.C., Fox, P.M., Mackay, C.E., Filippini, N., Watkins, K.E., Toro, R., Laird, A.R., and Beckmann, C.F. (2009). Correspondence of the brain's functional architecture during activation and rest. Proc. Natl. Acad. Sci. USA 106, 13040-13045.

Sporns, O., and Betzel, R.F. (2016). Modular brain networks. Annu. Rev. Psychol. 67, 613-640.

Sylvester, C.M., Yu, Q., Srivastava, A.B., Marek, S., Zheng, A., Alexopoulos, D., Smyser, C.D., Shimony, J.S., Ortega, M., Dierker, D.L., et al. (2020). Individual-specific functional connectivity of the amygdala: A substrate for precision psychiatry. Proc. Natl. Acad. Sci. USA 117, 3808-3818.

Tewarie, P., Hillebrand, A., van Dijk, B.W., Stam, C.J., O'Neill, G.C., Van Mieghem, P., Meier, J.M., Woolrich, M.W., Morris, P.G., and Brookes, M.J. (2016). Integrating cross-frequency and within band functional networks in restingstate MEG: A multi-layer network approach. Neuroimage 142, 324-336.

Thomas Yeo, B.T., Krienen, F.M., Sepulcre, J., Sabuncu, M.R., Lashkari, D., Hollinshead, M., Roffman, J.L., Smoller, J.W., Zöllei, L., Polimeni, J.R., et al. (2011). The organization of the human cerebral cortex estimated by intrinsic functional connectivity. J. Neurophysiol. 106, 1125-1165.

Thomas Yeo, B.T., Krienen, F.M., Chee, M.W., and Buckner, R.L. (2014). Estimates of segregation and overlap of functional connectivity networks in the human cerebral cortex. Neuroimage 88, 212-227.

Traag, V.A., Van Dooren, P., and Nesterov, Y. (2011). Narrow scope for resolution-limit-free community detection. Phys. Rev. E Stat. Nonlin. Soft Matter

Treiber, J.M., White, N.S., Steed, T.C., Bartsch, H., Holland, D., Farid, N., McDonald, C.R., Carter, B.S., Dale, A.M., and Chen, C.C. (2016). Characterization and correction of geometric distortions in 814 diffusion weighted images. PLoS ONE 11, e0152472.

Tustison, N.J., Avants, B.B., Cook, P.A., Zheng, Y., Egan, A., Yushkevich, P.A., and Gee, J.C. (2010). N4ITK: improved N3 bias correction. IEEE Trans. Med. Imaging 29, 1310-1320.

Uddin, L.Q. (2020). An 'edgy' new look. Nat. Neurosci. 23, 1471-1472.

Uddin, L.Q., Thomas Yeo, B.T., and Spreng, R.N. (2019). Towards a universal taxonomy of macro-scale functional human brain networks. Brain Topogr. 32,

Vaiana, M., and Muldoon, S.F. (2020). Multilayer brain networks. J. Nonlinear Sci. 30, 1-23,

Váša, F., Seidlitz, J., Romero-Garcia, R., Whitaker, K.J., Rosenthal, G., Vértes, P.E., Shinn, M., Alexander-Bloch, A., Fonagy, P., Dolan, R.J., et al.; NSPN constants and the state of thesortium (2018). Adolescent tuning of association cortex in human structural brain networks. Cereb. Cortex 28, 281-294.

Wang, S., Peterson, D.J., Gatenby, J.C., Li, W., Grabowski, T.J., and Madhyastha, T.M. (2017). Evaluation of field map and nonlinear registration methods for correction of susceptibility artifacts in diffusion MRI. Front. Neuro-

Wang, H.-T., Smallwood, J., Mourao-Miranda, J., Xia, C.H., Satterthwaite, T.D., Bassett, D.S., and Bzdok, D. (2020). Finding the needle in a high-dimensional haystack: Canonical correlation analysis for neuroscientists. Neuroimage 216, 116745.

Woo, C.-W., and Wager, T.D. (2015). Neuroimaging-based biomarker discovery and validation. Pain 156, 1379-1381.

Zalesky, A., Fornito, A., Cocchi, L., Gollo, L.L., and Breakspear, M. (2014). Time-resolved resting-state brain networks. Proc. Natl. Acad. Sci. USA 111, 10341-10346

Zamani Esfahlani, F., Bertolero, M.A., Bassett, D.S., and Betzel, R.F. (2020a). Space-independent community and hub structure of functional brain networks. Neuroimage 211, 116612.

Zamani Esfahlani, F., Byrge, L., Tanner, J., Sporns, O., Kennedy, D., and Betzel, R. (2021a). Edge-centric analysis of time-varying functional brain networks with applications in autism spectrum disorder. bioRxiv. https://doi.org/10. 1101/2021.07.01.450812.

Zamani Esfahlani, F., Jo, Y., Faskowitz, J., Byrge, L., Kennedy, D., Sporns, O., and Betzel, R. (2020b). High-amplitude co-fluctuations in cortical activity drive functional connectivity. bioRxiv, 800045.

Zamani Esfahlani, F., Jo, Y., Puxeddu, M.G., Merritt, H., Tanner, J.C., Greenwell, S., Patel, R., Faskowitz, J., and Betzel, R.F. (2021b). Modularity maximization as a flexible and generic framework for brain network exploratory analysis. Neuroimage 244, 118607, arXiv:2106.15428.

Zhang, Y., Brady, M., and Smith, S. (2001). Segmentation of brain MR images through a hidden Markov random field model and the expectation-maximization algorithm. IEEE Trans. Med. Imaging 20, 45-57.

Zuo, X.-N., He, Y., Betzel, R.F., Colcombe, S., Sporns, O., and Milham, M.P. (2017). Human connectomics across the life span. Trends Cogn. Sci. 21, 32-45.





STAR*METHODS

KEY RESOURCES TABLE

REAGENT or RESOURCE	SOURCE	IDENTIFIER
Deposited Data		
Midnight Scan Club raw data	Gordon et al. (2017b)	https://openneuro.org/datasets/ds000224/versions/00002 Openneuro
Software and Algorithms		
MATLAB	Mathworks	RRID: SCR_001622 https://www.mathworks.com/
Brain Connectivity Toolbox	Rubinov & Sporns (2010)	RRID: SCR_004841 https://sites.google.com/site/bctnet/
fMRIPrep	Esteban et al. (2018)	RRID: SCR_016216 https://fmriprep.org/en/stable/
NiLearn	Abraham et al. (2014)	RRID: SCR_001362 http://nilearn.github.io
Advanced Normalization Tools	Avants et al. (2009)	RRID: SCR_004757 http://picsl.upenn.edu/software/ants
Freesurfer	Dale et al. (1999)	RRID: SCR_001847 https://surfer.nmr.mgh.harvard.edu/
FSL	Smith et al. (2004)	RRID: SCR_002823 https://fsl.fmrib.ox.ac.uk/fsl/fslwiki
AFNI	Cox (1996)	RRID: SCR_005927 https://afni.nimh.nih.gov/afni/
Generalized Louvain algorithm	Jutla et al. (2011)	http://netwiki.amath.unc.edu/GenLouvain/GenLouvain

RESOURCE AVAILABILITY

Lead contact

Further information and requests for resources and reagents should be directed to and will be fulfilled by the lead contact, Richard Betzel (rbetzel@indiana.edu).

Material availability

This study generated no new reagents or materials. See following section for Data and code availability.

Data and code availability

- MRI data are deposited and publicly available in the OpenNeuro data repository (https://openneuro.org/datasets/ds000224/ versions/00002). The accession number is OpenNeuro: ds000224.
- Code to transform fMRI time courses into edge time series, construct edge functional connectivity, detect edge communities, and compute edge community profile similarity is available at https://github.com/brain-networks/edge-centric_demo.
- Any additional information required to reanalyze the data reported in this paper is available from the lead contact upon request.

EXPERIMENTAL MODEL AND SUBJECT DETAILS

The Midnight Scan Club (MSC) dataset (Gordon et al., 2017b) included rsfMRI from 10 adults (50% female, mean age = 29.1 ± 3.3, age range = 24-34). The study was approved by the Washington University School of Medicine Human Studies Committee and Institutional Review Board and informed consent was obtained from all subjects. These data were initially reported in Gordon et al. (2017a).

METHOD DETAILS

Functional preprocessing

Subjects underwent 12 scanning sessions on separate days, each session beginning at midnight. Ten (10) rsfMRI scans per subject were collected with a gradient-echo EPI sequence (run duration = 30 min, TR = 2200 ms, TE = 27 ms, flip angle = 90°, 4 mm isotropic voxel resolution) with eyes open and with eye tracking recording to monitor for prolonged eye closure (to assess drowsiness). Images were collected on a 3T Siemens Trio. Functional images in the MSC dataset were preprocessed using fMRIPrep 1.3.2 (Esteban et al., 2018), which is based on Nipype 1.1.9 (Gorgolewski et al., 2011). The following description of fMRIPrep's preprocessing is based on boilerplate distributed with the software covered by a "no rights reserved" (CC0) license. Internal operations of fMRIPrep use Nilearn

Article



0.5.0 (Abraham et al., 2014), ANTs 2.2.0 (Avants et al., 2009), FreeSurfer 6.0.1 (Dale et al., 1999), FSL 5.0.9 (Smith et al., 2004), and AFNI v16.2.07 (Cox, 1996). For more details about the pipeline, see the section corresponding to workflows in fMRIPrep's documentation.

The T1-weighted (T1w) image was corrected for intensity non-uniformity with N4BiasFieldCorrection (Tustison et al., 2010; Avants et al., 2008), distributed with ANTs, and used as T1w-reference throughout the workflow. The T1w-reference was then skull-stripped with a Nipype implementation of the antsBrainExtraction.sh workflow. Brain surfaces were reconstructed using recon-all (Dale et al., 1999), and the brain mask estimated previously was refined with a custom variation of the method to reconcile ANTs-derived and FreeSurfer-derived segmentations of the cortical gray-matter using Mindboggle (Klein et al., 2017). Spatial normalization to the ICBM 152 Nonlinear Asymmetrical template version 2009c (Fonov et al., 2009) was performed through nonlinear registration with antsRegistration, using brain-extracted versions of both T1w volume and template. Brain tissue segmentation of cerebrospinal fluid (CSF), white-matter (WM) and gray-matter (GM) was performed on the brain-extracted T1w using FSL's fast (Zhang et al., 2001).

Functional data was slice time corrected using AFNI's 3dTshift and motion corrected using FSL's mcflirt (Jenkinson et al., 2002). Fieldmap-less distortion correction was performed by co-registering the functional image to the same-subject T1w image with intensity inverted (Wang et al., 2017) constrained with an average fieldmap template (Treiber et al., 2016), implemented with antsRegistration. This was followed by co-registration to the corresponding T1w using boundary-based registration (Greve and Fischl, 2009) with 9 degrees of freedom. Motion correcting transformations, field distortion correcting warp, BOLD-to-T1w transformation and T1w-to-template (MNI) warp were concatenated and applied in a single step using antsApplyTransforms using Lanczos interpolation. Several confounding time-series were calculated based on this preprocessed BOLD: framewise displacement (FD), DVARS and three region-wise global signals. FD and DVARS are calculated for each functional run, both using their implementations in Nipype (Power et al., 2014). The three global signals are extracted within the CSF, the WM, and the whole-brain masks. The resultant NIFTI file for each MSC subject used in this study followed the file naming pattern *_space-T1w_desc-preproc_bold.nii.gz.

Image quality control

The quality of functional images in the MSC were assessed using fMRIPrep's visual reports and MRIQC 0.15.1 (Esteban et al., 2017). Data was visually inspected for whole brain field of view coverage, signal artifacts, and proper alignment to the corresponding anatomical image.

QUANTIFICATION AND STATISTICAL ANALYSIS

Parcellation preprocessing

A functional parcellation designed to optimize both local gradient and global similarity measures of the fMRI signal (Schaefer et al., 2017) (Schaefer400) was used to define 400 areas on the cerebral cortex. These nodes are also mapped to the Thomas Yeo et al. (2011) canonical functional networks. For the MSC dataset, a Schaefer400 parcellation was obtained for each subject using a Gaussian classifier surface atlas (Fischl et al., 2004) (trained on 100 unrelated Human Connectome Project subjects) and FreeSurfer's mris_ca_label function. These tools utilize the surface registrations computed in the recon-all pipeline to transfer a group average atlas to subject space based on individual surface curvature and sulcal patterns. This method rendered a T1w space volume for each subject. For use with functional data, the parcellation was resampled to 2mm T1w space.

Functional network preprocessing

Each preprocessed BOLD image was linearly detrended, band-pass filtered (0.008-0.08 Hz) (Parkes et al., 2018), confound regressed and standardized using Nilearn's signal.clean, which removes confounds orthogonally to the temporal filters (Lindquist et al., 2019). The confound regression employed (Satterthwaite et al., 2013) included 6 motion estimates, time series of the mean CSF, mean WM, and mean global signal, the derivatives of these nine regressors, and the squares these 18 terms. Furthermore, a spike regressor was added for each frame exceeding 0.5mm framewise displacement. Following preprocessing and nuisance regression, residual mean BOLD time series at each node were recovered. eFC matrices for each subject were computed and then averaged across subjects, to obtain a representative eFC matrix for each dataset.

Edge graph construction

Constructing networks from fMRI data (or any neural time series data) requires estimating the statistical dependency between pairs of time series. The magnitude of that dependency is usually interpreted as a measure of how strongly (or weakly) those voxels are parcels are functionally connected to each other. By far the most common measure of statistic dependence is the Pearson correlation coefficient. Let $\mathbf{x}_i = [x_i(1), ..., x_i(T)]$ and $\mathbf{x}_i = [x_i(1), ..., x_i(T)]$ be the time series recorded from voxels or parcels i and j, respectively. We can calculate the correlation of i and j by first z-scoring each time series, such that $\mathbf{z}_i = (\mathbf{x}_i - \mu_1)/\sigma_i$, where $\mu_i = 1/T \sum_i x_i(t)$ and $\sigma_i = 1/(T-1)\sum_t [x_i(t) - \mu_i]$ are the time-averaged mean and standard deviation. Then, the correlation of i with j can be calculated as: $r_{ij} = 1/(T-1)\sum_{t}[z_i(t)\cdot z_j(t)]$. Repeating this procedure for all pairs of parcels results in a node-by-node correlation matrix, i.e., an estimate of FC. If there are N nodes, this matrix has dimensions $[N \times N]$.

To estimate edge-centric networks, we need to modify the above approach in one small but crucial way. Suppose we have two z-scored parcel time series, z_i and z_i . To estimate their correlation we calculate the mean their element-wise product (not exactly



the average, because we divide by T-1 rather than T). Suppose, instead, that we never calculate the mean and simply stop after calculating the element-wise product. This operation would result in a vector of length T whose elements encode the moment-bymoment co-fluctuations magnitude of parcels i and j. For instance, suppose at time t, parcels i and j simultaneously increased their activity relative to baseline. These increases are encoded in z_i and z_i as positive entries in the th position, so their product is also positive. The same would be true if i and j decreased their activity simultaneously (because the product of negatives is a positive). On the other hand, if i increased while j decreased (or vice versa), this would manifest as a negative entry. Similarly, if either i or j increased or decreased while the activity of the other was close to baseline, the corresponding entry would be close to zero.

Accordingly, the vector resulting from the element-wise product of \mathbf{z}_i and \mathbf{z}_i can be viewed as encoding the magnitude of momentto-moment co-fluctuations between i and j. An analogous vector can easily be calculated for every pair of parcels (network nodes), resulting in a set of co-fluctuation (edge) time series. With N parcels, this results in (N(N-1)/2) pairs, each of length T. From these time series we can estimate the statistical dependency for every pair of edges. We refer to this construct as edge functional connectivity (eFC). Let $\mathbf{c}_{ij} = [z_i(1) \cdot z_j(1), ..., z_i(T) \cdot z_j(T)]$ and $\mathbf{c}_{uv} = [z_u(1) \cdot z_v(1), ..., z_i(T) \cdot z_j(T)]$ be the time series for edges $\{i, j\}$ and $\{u, v\}$, respectively. Then we can calculate eFC as:

$$eFC_{ij,uv} = \frac{\sum_{t} c_{ij}(t) \cdot c_{uv}(t)}{\sqrt{\sum_{t} c_{ij}(t)^{2}} \sqrt{\sum_{t} c_{uv}(t)^{2}}}.$$
 (Equation 1)

Here, the denominator is necessary to bound eFC to the interval [-1,1].

Edge community detection algorithm

In our previous paper we developed a spectral method for clustering eFC matrices (Faskowitz et al., 2020). Although this algorithm operated on a reduced rank version of eFC matrices, obtaining these lower rank data required first generating the eFC matrix. In general, eFC matrices are much larger than nFC matrices. This means that they take longer to compute and much more memory. Here, we circumvent this issue by clustering the edge time series directly. A parcellation of the brain into N regions results in M =[N(N-1)]/2 edges. So rather than generating an $M \times M$ matrix, reducing its dimensionality, and then clustering its low-dimensional representation, we simply cluster the $M \times T$ time series (where T) is the number of samples. We use a k-means clustering algorithm where the distance metric is defined as (1 - eFC)/2. Two perfectly correlated edge time series have a distance of 0 while two orthogonal edge time series would have a distance of 1.

We used this same algorithm to generate estimates of edge communities at the scale of scans, subjects, and cohort. To generate subject-representative communities, we concatenated edge time series from all of a subjects' scans and clustered the concatenated time series. Similarly, to generate group representative partitions, we concatenated scans from all subjects. At all scales, we repeated the clustering algorithm 250 times.

To ensure that 250 repetitions were sufficient for sampling the space of possible partitions, we performed the following analysis. First, we calculated the cluster co-assignment matrix using all 250 partitions. The co-assignment matrix has dimensions $M \times M$ and its elements encode how many times two edges were assigned to the same cluster out of the 250 total partitions. Next, we generated co-assignment matrices using random sub-samples of those 250 partitions. We tested sample sizes ranging from 5 to 100 in increments of 5. For each sample, we computed the similarity (correlation) of its corresponding co-assignment matrix with the elements of the co-assignment matrix estimated from the full sample of 250 partitions. For k = 10 clusters, we found that with as few as 25 samples, the similarity between co-assignment matrices was already $r = 0.991 \pm 10^{-5}$. These observations suggest that k-means quickly converges to a small set of solutions. Moreover, it suggests that the 250 repeats was likely sufficient for obtaining a meaningful sample of the space of possible partitions.

Community overlap metrics

The clustering algorithm partitioned edges into non-overlapping clusters. That is, every edge $\{i,j\}$, where $i,j \in \{1,...,N\}$, was assigned to one of k clusters. In this list of edges, each node appeared N-1 times (we excluded self-connections). Region i's participation in cluster c was calculated as:

$$\rho_{ic} = \frac{1}{N-1} \sum_{i \neq i} \delta(g_{ij}, \mathbf{c})$$
 (Equation 2)

where $g_{ii} \in \{1, ..., k\}$ was the cluster assignment of the edge linking nodes i and j and $\delta(x, y)$ is the Kronecker delta, whose value is 1 if x = y and zero otherwise.

By definition, $\sum p_{ic} = 1$, and we can treat the vector $\mathbf{p}_i = [p_{i1}, \dots, p_{ik}]$ as a probability distribution. The entropy of this distribution measures the exfent to which region i's community affiliations are distributed evenly across all communities (high entropy and high overlap) or concentrated within a small number of communities (low entropy and low overlap). We calculate this entropy as:

$$h_i = -\sum_c p_{ic} \log_2 p_{ic}.$$
 (Equation 3)



To normalize this measure and bound it to the interval [0, 1], we divide by log₂k. We refer to this measure as community entropy and interpret this value as an index of overlap.

Edge community similarity

When we cluster an eFC matrix, we assign each edge to a single community. These edge communities can be rearranged into the upper triangle of a $N \times N$ matrix, **X**, whose element x_{ij} denotes the edge community assignment of the edge between nodes i and j. The ith column of **X**, which we denote as $\mathbf{x}_i = [x_{1i}, \dots, x_{Ni}]$, encodes the community labels of all edges in which node i participates. Note that we do not consider self-edges, so the element x_{ii} is left empty.

From this matrix, we can compare the edge communities of nodes i and j by calculating the similarity of vectors \mathbf{x}_i and \mathbf{x}_i . Here, we measure that similarity as the fraction of elements in both vectors with the same community label. That is:

$$s_{ij} = \frac{1}{N-2} \sum_{u \neq i} \delta(x_{iu}, x_{ju})$$
 (Equation 4)

Here, $\delta(x,y)$ is the Kronecker delta, and takes on a value of 1 when x and y have the same value, but is zero otherwise. Note that the scaling factor is N-2 because we ignore the self-connections x_{ij} and x_{jj} . Repeating this comparison for all pairs of nodes generates the similarity matrix, $\mathbf{S} = \{s_{ii}\}.$

Modularity maximization

In the main text, we computed system and whole-brain edge community similarity matrices. To discover the meso-scale structure of these matrices we used a multi-scale modularity maximization algorithm (Newman and Girvan, 2004; Traag et al., 2011; Bazzi et al., 2016). Modularity maximization detects meso-scale structure according to a simple principle: clusters are groups of nodes whose actual connection weight is greater than what we would expect by chance. This general framework is flexible and, through parameterization can be used to detect clusters of different sizes (Reichardt and Bornholdt, 2006) and across layers (time (Bassett et al., 2013), subjects (Betzel et al., 2019a), frequencies (Tewarie et al., 2016)).

Formally, the modularity quality function is expressed as:

$$Q(\gamma) = \sum_{ij} [A_{ij} - \gamma \cdot P_{ij}] \delta(\sigma_i, \sigma_j)$$
 (Equation 5)

where A_{ij} is the observed weight of connections between nodes i and j, P_{ij} is the expected weight under some null model, γ is a structural resolution parameter, and $\delta(x,y)$ is the Kronecker delta and is equal to 1 when the community assignments of nodes i and j, denoted as σ_i and σ_i , respectively, are identical and is equal to 0 otherwise. The inclusion of the delta function means that the double summation is over node pairs that fall within communities. Thus, $Q(\gamma)$ measures the total weight of within-community connections less their expected values. The modularity maximization framework seeks to maximize the value of $Q(\gamma)$ by selecting nodes' community assignments.

Here we used a uniform null model, i.e., $P_{ij} = 1$ for all node pairs. Combined with the resolution parameter, γ , communities detected under this null model represent groups of nodes whose average similarity of edge community profiles exceeds γ. Note that we selected this particular null model deliberately, as previous studies have shown that it is especially well-suited for networks whose weights reflect statistical measures of similarity or correlation (Traag et al., 2011; Bazzi et al., 2016). We further note that this null model has been used in previous studies (Betzel et al., 2019b; Zamani Esfahlani et al., 2020a; Betzel, 2018; Kenett et al., 2020; Betzel et al., 2017).

In more detail, we selected 200 values of γ , linearly-spaced over the interval [0, 1]. At each value, we ran a Louvain-like algorithm to optimize modularity (Jutla et al., 2011; Blondel et al., 2008). Because this optimization algorithm is non-deterministic, we performed 50 iterations at each value of γ . We then aggregated γ values into 10 linearly-spaced intervals and, within each interval, used to detected clusters to generate a single representative set of clusters using a consensus clustering algorithm (Lancichinetti and Fortunato, 2012; Rubinov and Sporns, 2010). Briefly, this algorithm involved estimating the co-assignment matrix from the detected clusters, whose elements indicate the fraction of times that nodes i and j were assigned to the same cluster across all partitions within that interval. We then calculated the expected fraction (by randomly permuting nodes' community assignments independently for each partition). The observed and expected co-assignment values can be used to define a consensus modularity function that we optimized using the same Louvain-like algorithm (1000 repetitions). If any of the 1000 partitions were dissimilar, we recomputed a co-assignment matrix and the expected co-assignment and repeated the algorithm. These two steps - calculation of co-assignment values and clustering - were repeated until convergence, i.e., all detected partitions are identical. In practice, the algorithm converged in three or fewer iterations.

Edge community segregation

In the main text, we described a procedure in which we imposed edge community structure onto eFC matrices and measured a quantity that we referred to as an index of "segregation." To calculate the segregation index, we measured two quantities induced by edge





 $communities: \textit{eFC}_{within} \text{ and } \textit{eFC}_{between}, \text{ which measure the average eFC weight within and between edge communities. The segre$ gation index, then, is simply the difference in these two quantities:

Segregation =
$$eFC_{within} - eFC_{between}$$
. (Equation 6)

Because we define edge communities to be groups of edges with similar co-fluctuation patterns, we expect eFCwithin

Differential identifiability

Suppose we had a dataset comprising many scans from many subjects. We would say that subjects are "identifiable" if, given a scan's worth of data from one subject, we could accurately identify other scans from the same subject (Finn et al., 2015). This intuition can be formalized using the measure differential identifiability (Amico and Goñi, 2018):

$$I_{\text{diff}} = I_{\text{within}} - I_{\text{between}}.$$
 (Equation 7)

In this expression I_{within} and I_{between} are the mean similarities among scans from the same and different subjects. Here, we measure similarity as the Pearson correlation between regions' edge community similarity vectors. Thus, I_{diff} measures how much more similar subjects are to themselves then they are to other subjects.